

**DETrital ZIRCON INVESTIGATION INTO THE LATE  
PROTEROZOIC TO EARLY PALEozoic TECTONIC HISTORY  
OF THE QING SHAN REGION OF THE NAN SHAN, NORTHEAST  
TIBET**

---

**A Thesis**

**Presented to**

**the Faculty of the Department of Earth and Atmospheric Sciences**

**University of Houston**

---

**In Partial Fulfillment**

**of the Requirements for the Degree**

**Master of Science**

---

**By**

**Serdar Bektas**

**December, 2013**

**DETrital ZIRCON INVESTIGATION INTO THE LATE  
PROTEROZOIC TO EARLY PALEozoic TECTONIC HISTORY OF  
THE QING SHAN REGION OF THE NAN SHAN, NORTHEAST  
TIBET**

---

Serdar Bektas

APPROVED

---

Dr. Alexander Robinson, Chairman

---

Prof. Hua-Wei Zhou

---

Dr. Thomas J. Lapen

---

Dr. Jerome Guynn

---

Dean, College of Natural Sciences and  
Mathematics

## **ACKNOWLEDGEMENTS**

I would like to specially thank Dr. Alexander Robinson for presenting me the opportunity and for his continued support, guidance, and patience throughout this project. My sincerest gratitude goes to Mr. Barry J. Shaulis and Mr. Adrian S. Gittens for taking the time and teaches me the relevant techniques required for zircon processing and analysis and general suggestions and conversation. Finally, I would like to thank my family, especially my wife Isabel Raciny Bektas, and my daughter for their continued support and encouragement.

**DETTRITAL ZIRCON INVESTIGATION INTO THE LATE  
PROTEROZOIC TO EARLY PALEOZOIC TECTONIC HISTORY OF  
THE QING SHAN REGION OF THE NAN SHAN, NORTHEAST  
TIBET**

---

**A Thesis**

**Presented to**

**the Faculty of the Department of Earth and Atmospheric Sciences**

**University of Houston**

---

**In Partial Fulfillment**

**of the Requirements for the Degree**

**Master of Science**

---

**By**

**Serdar Bektas**

**December,2013**

## ABSTRACT

The northeastern Tibetan Plateau consists of the Qilian Shan, Nan Shan, and Qiadam terranes. This region has been extensively studied due to its complicated tectonic history, and has yielded different tectonic models for the Late Proterozoic to Early Paleozoic. These models include the Archipelago model, the North-facing Magmatic Arc model, and more complicated models such as the Multiple-accretionary and the Back-arc extension models. These models propose that the region was formed by various oceanic basin subductions and collisions between the different terranes. In contrast, the Broad Convergent model proposes that the terrane assemblages which grew progressively southwestward by addition of accretionary complexes and magmatic arcs. However, there is no consensus about subduction polarities, and tectonic formation of region. Analysis of detrital zircon from these terranes provides a potential opportunity to differentiate between some of these models.

In order to address the tectonic evolution of the southern Nan Shan, I conducted U-Pb detrital zircon analyses on five samples of Proterozoic to Early Paleozoic lithologies in the Qing Shan mountains at the southern margin of the Nan Shan-Qilian Shan region. One sample from a Proterozoic unit yields a strong Neoproterozoic age population (~800 Ma) and might represent the regional basement or local igneous sources that resulted from rifting of continental crust. This sample reveals that the basement beneath Qing Shan is as old as late Proterozoic. This result is consistent with the North-facing Magmatic Arc model, the Archipelago, and the Multiple-accretionary model, since the

models suggest that the basement age of the Nan Shan region consists of late Proterozoic units. Zircon grains from the Proterozoic sample may have been derived from magmatism related to the breakup of Rodinia due to their mafic origin.

All other samples yielded Early Paleozoic (Ordovician to Silurian) maximum depositional ages, and broadly similar age distributions. The Early Paleozoic detrital zircon ages are interpreted to be derived from arc magmatism, as most of the grains yield an igneous U/Th signature. These ages might be related to the southward subduction of the North Qilian Ocean beneath the Qilian Shan, which is consistent with the North-facing Magmatic Arc model, or northward subduction of an ocean basin between the Qaidam and the Nan Shan terranes during the Late Cambrian to Early Silurian, which is consistent with the Archipelago and Multiple-accretionary models.

## **TABLE OF CONTENTS**

<b>CHAPTER 1</b>	<b>INTRODUCTION</b>	<b>1</b>
<b>1.1</b>	<b>GEOLOGIC BACKGROUND</b>	<b>2</b>
	<b>    1.1.1 TECTONIC HISTORY OF REGION</b>	<b>6</b>
	<b>        1.1.1.1 Archipelago Model</b>	<b>6</b>
	<b>        1.1.1.2 Multiple-accretionary Model</b>	<b>7</b>
	<b>        1.1.1.3 Broad Convergent Model</b>	<b>8</b>
	<b>        1.1.1.4 The Northeast-facing Magmatic Arc Model</b>	<b>9</b>
	<b>        1.1.1.5 Back-arc Convergent Model</b>	<b>10</b>
<b>1.2</b>	<b>STRATIGRAPHY OF THE QING SHAN</b>	<b>11</b>
<b>CHAPTER 2</b>	<b>METHODS</b>	<b>17</b>
<b>2.1</b>	<b>SAMPLE PREPARATION</b>	<b>17</b>
<b>2.2</b>	<b>ANALYTICAL METHODS</b>	<b>17</b>
	<b>    2.2.1 ASER ABLATION INDUCTIVELY COUPLED MASS SPECTOMETRY</b>	<b>17</b>
	<b>    2.2.2 DATA ACQUISITION AND REDUCTION</b>	<b>17</b>
	<b>    2.2.3 ISOTOPE SYSTEM</b>	<b>19</b>
<b>CHAPTER 3</b>	<b>RESULTS</b>	<b>21</b>
<b>3.1</b>	<b>SAMPLE DATA</b>	<b>21</b>
	<b>    3.1.1 5-30-02-1</b>	<b>21</b>
	<b>    3.1.2 5-30-02-3A</b>	<b>23</b>
	<b>    3.1.3 7-01-02-10</b>	<b>25</b>
	<b>    3.1.4 6-27-02-11</b>	<b>27</b>

<b>3.1.5 6-29-07-3</b>	<b>29</b>
<b>3.2 DISCUSSION</b>	<b>32</b>
<b>3.2.1 POTENCIAL SOURCES</b>	<b>32</b>
<b>3.2.2 5-30-02-1</b>	<b>34</b>
<b>3.2.3 5-30-02-3A</b>	<b>34</b>
<b>3.2.4 7-01-02-10</b>	<b>35</b>
<b>3.2.5 6-29-07-3</b>	<b>35</b>
<b>3.2.6 6-27-02-11</b>	<b>36</b>
<b>3.3 TECTONIC MODELS</b>	<b>36</b>
<b>CHAPTER 4 CONCLUSION</b>	<b>41</b>
<b>References Cited</b>	<b>42</b>
<b>Appendix A.1</b>	<b>45</b>
<b>Appendix B.1</b>	<b>48</b>
<b>Appendix C.1</b>	<b>52</b>
<b>Appendix D.1</b>	<b>55</b>
<b>Appendix E.1</b>	<b>59</b>

## CHAPTER 1

### 1. INTRODUCTION

The northeastern Tibetan Plateau is composed of the Qilian Shan, Nan Shan, and Qiadam terranes which are a collage of tectonic assemblages that formed in different tectonic environments (Figure 1). While the tectonic history of this region and surrounding terranes have been extensively researched, significant uncertainty remains regarding their history. Previous studies have proposed various tectonic scenarios involving arc-continent collisions, continent-continent collision, and continent-oceanic collision. However, there is still no consensus regarding the tectonic history of the region during the Late Proterozoic to Early Paleozoic, especially in regards to subduction polarities, basement age beneath the Qilian Shan- Nan Shan terranes, and tectonic formation of the region.

Previous work on a thick sequence of metaturbidites in the northwestern Nan Shan region by Gehrels et al. (2003) documented dominant detrital-zircon ages ca.  $823 \pm 16$  Ma and older grains ranging from 2.7 Ma and 2.3 Ma. Liu et al. (1988) assigned the sequence an Early Paleozoic age. Based on the ages, they were suggested to have been sourced from Australia, North China, or South China. Further, Gehrels et al. analyzed detrital zircons from a Proterozoic quartz-rich metaturbidite sequence from the Nan Shan, which contains mainly ~800 Ma grains and subordinate >1.8 Ga grains. The ~800 Ma grains were interpreted to be derived from metaplutonic and metavolcanic arc (?) assemblages that form the basement of the Early Paleozoic arc system. Finally, Gehrels et al., (2011) interpreted detrital zircons in Upper Proterozoic and Lower Paleozoic units to be shed

from convergent margin systems preserved within the East African Orogen and Ross-Delamarian Orogen of Gondwana.

My research focuses on addressing tectonic models for the region using U/Pb geochronologic analyses of detrital zircon grains by LA-ICPMS, obtained from Proterozoic to Devonian units. My results are used to: (1) shed light on the tectonic history of the region, and (2) address basement ages of the Qing Shan and Nan Shan terrain.

### 1.1 GEOLOGIC BACKGROUND

The Qing Shan is located in the northeastern part of the Tibetan Plateau at the southern margin of the Nan Shan-Qilian Shan terranes. It is bounded by the Alashan Block, the North Qilian orogenic belt, and the Central Qilian Block to the north, and the North Qaidam continental-type Ultra High Pressure Metamorphic (UHPM) belt to the south (Figure 1). These units are truncated to the west by the NE-striking left-lateral Altyn Tagh Fault system which connects with thrust belts in the Nan Shan–Qilian Shan at its NE end. To the north, the Alashan Block has been interpreted to be the western part of the North China Craton, and is comprised of early Precambrian basement with 1.9 Ga granitic gneisses (Xiu et al., 2004). It has 1.7 - 2.7 Ga detrital zircon ages (Geng et al., 2007; Tung et al., 2007) and is overlain by Cambrian to middle Ordovician sequences (Bureau of Geology and Mineral Resources of Ningxia Province, 1990). The NW-SE-trending North Qilian orogenic belt is located between the Alashan Block to the north and the Central Qilian Shan to the south. The belt consists of Neoproterozoic to Early

Paleozoic ophiolite sequences, high-pressure metamorphic rocks, mafic/ultramafic rocks, Silurian flysch, Devonian molasse, and Carboniferous to Triassic sedimentary cover sequences (Song et al., 2012). Lawsonite-bearing metapelites have been recognized in the North Qilian orogenic belt supporting the interpretation that the North Qilian orogenic belt was formed by subduction of cold ocean crust. The Central Qilian Block is located between the North Qilian orogenic belt and the North Qaidam UHPM belt, and is interpreted as an imbricate thrust belt of Precambrian basement overlain by Paleozoic sedimentary sequences (Song et al., 2012). The basement consists predominantly of granitic gneiss, marble, amphibolite, and minor granulite. The North Qaidam continental-type UHPM belt is composed of eclogite, diamond-bearing lithologies, and garnet peridotite which were created along a north-dipping subduction zone by subduction of the North Qaidam continental crust to depths of > 90 km.

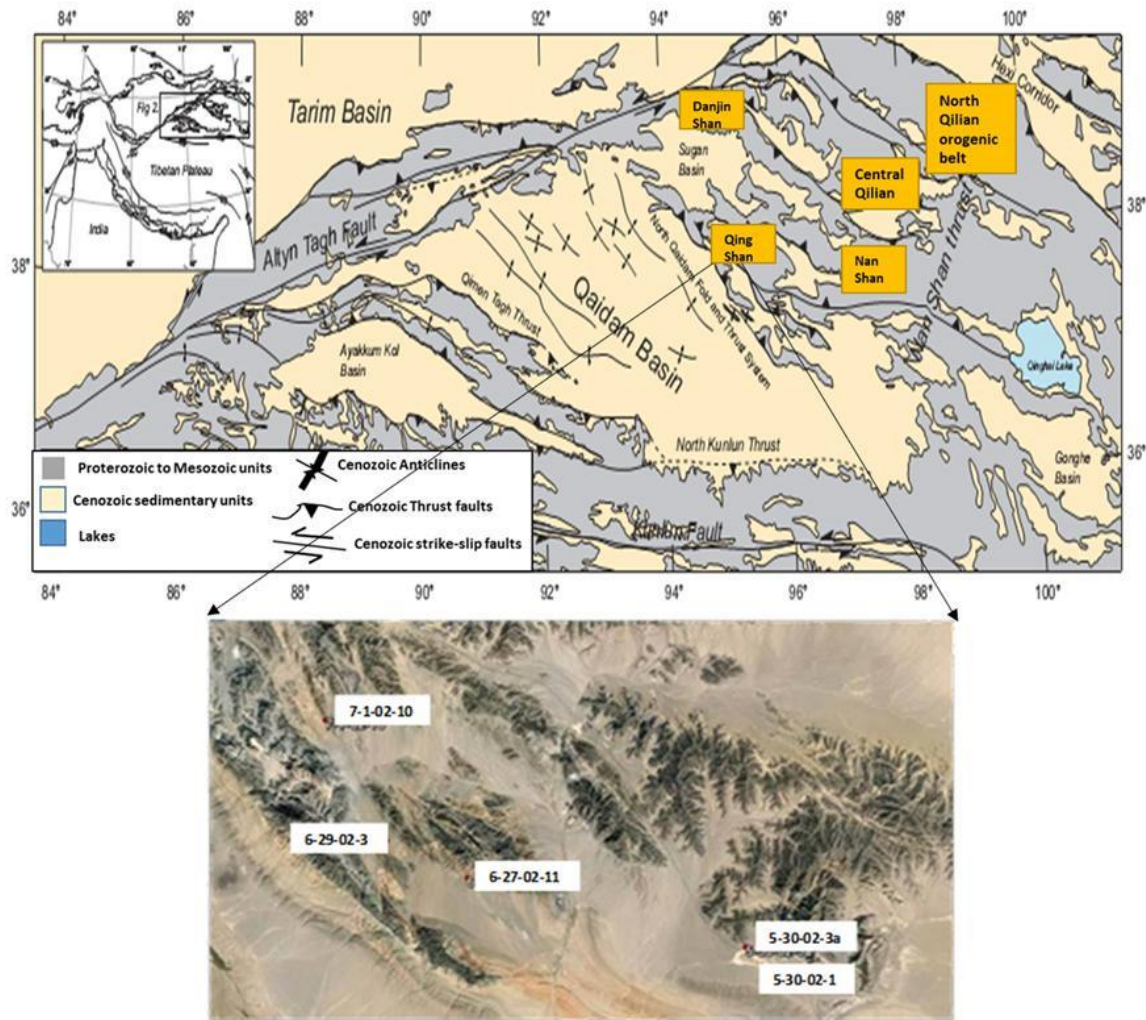
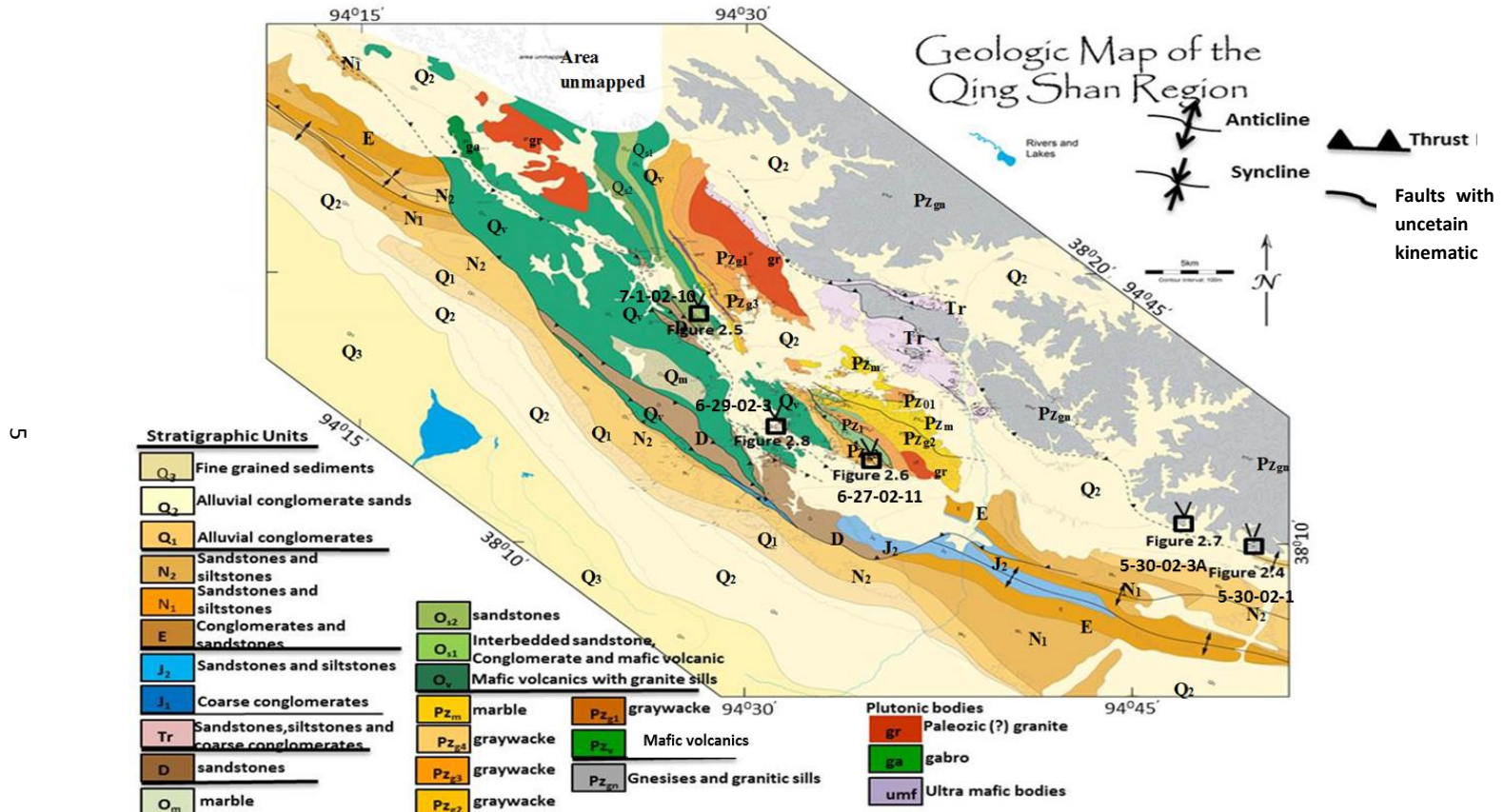


**Figure 1. A)** Map of the Himalayan-Tibetan orogeny showing the location of the study area in the northeastern part of the Tibetan plateau (Song et al., 2013). Digital topography from GLOBE project of the National Geophysical Data Center. **B)** Sample locations on a Google Earth image.



Modified after Robison et al., 2008

Figure 2. Geologic map of the Qing Shan region (Modified after Xiao et al., 2009).

### **1.1.1. Tectonic History of Region**

There are a wide range of competing models which suggest different tectonic histories for the formation of the region during the Late Proterozoic to Early Paleozoic. These models make different predictions of expected detrital age populations for Late Proterozoic to Early Paleozoic detrital sediments.

#### **1.1.1.1 Archipelago Model**

Li et al. (1978), Xiong and Coney et al. (1985), Hsu et al. (1995), Xia et al. (1996), and Yin and Harrison (2000) suggested the Qilian and the Qiadam oceanic and arc-type assemblages are composed of independent continental and volcanic island arcs that were separated by ocean basins during the Early Paleozoic (Figure 3).

According to the model, the Qilian Shan terrane can be separated into three belts: the North, Central, and South Qilian belts. The Central Qilian belt was separated from the southern margin of North China in the Late Proterozoic to Cambrian as a result of back-arc extension behind a north-dipping subduction zone (Xia et al., 1996). The northern Qilian belt is interpreted as an island arc system which was built along the southern margin of North China. Subduction resulted in collision between the northern Qilian Shan arc and the Central Qilian belt during the Early Devonian, although closure of the ocean basins may have been earlier during the Early Silurian or latest Ordovician.

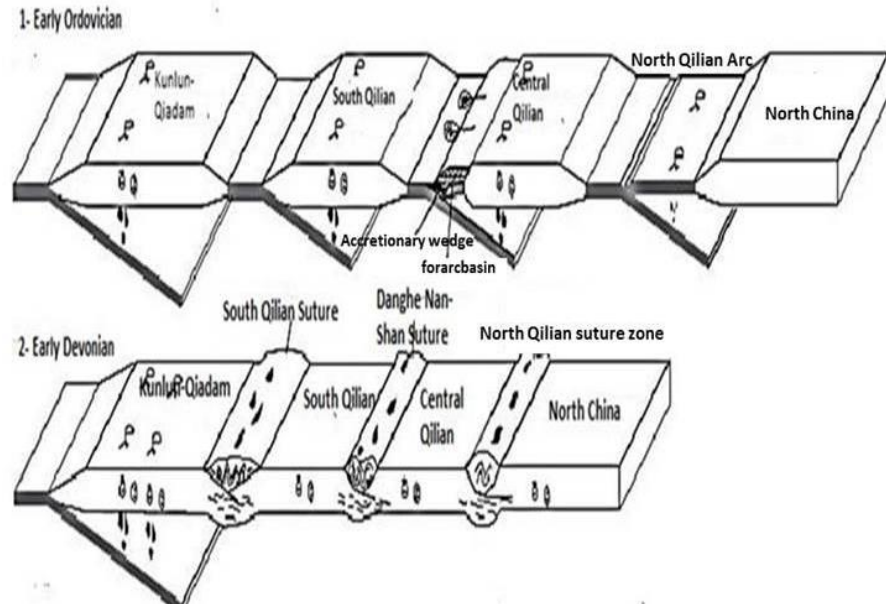


**Figure 3: Paleozoic tectonic evolution of the Northeastern Tibet (modified from Yin and Harrison et al., 2000).**

#### 1.1.1.2 Multiple-accretionary Model

The Multiple-accretionary model is a modification of the Archipelago model, with different predicted subduction zone polarities, and an extra arc not accounted for in the Archipelago model (Figure 4). These differences include coeval subduction of the Yushugou oceanic plate southward beneath the Central Qilian and northward beneath an island arc (North Qilian terrane), as well as southward subduction of the southern Alax terrane beneath the oceanic North Qilian terrane producing the Baiqanmen blueschist, ophiolite, and accretionary wedge deposit.

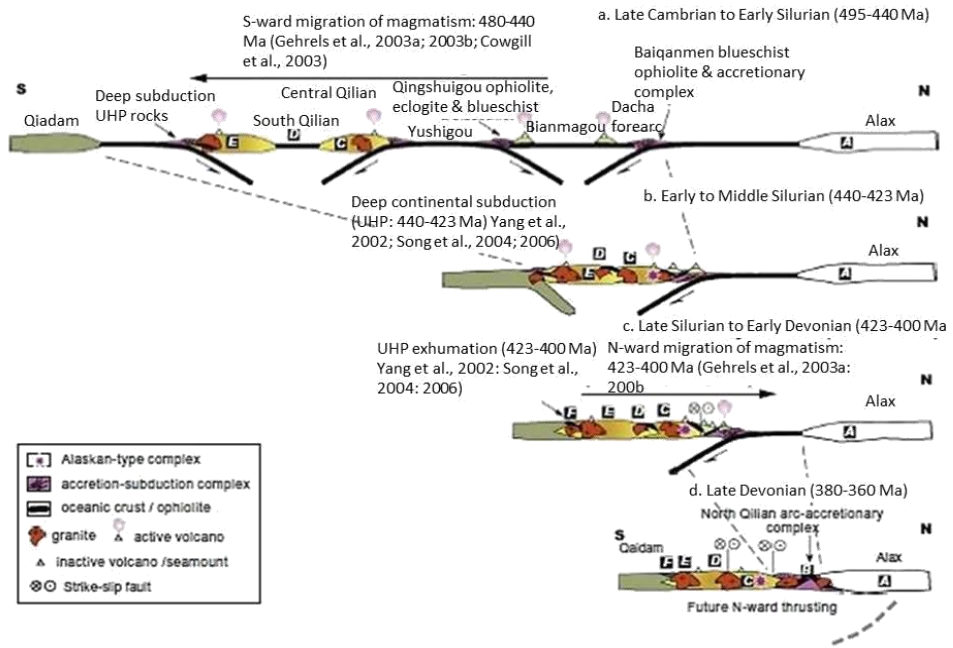


**Figure 4. Late Cambrian-Late Devonian tectonic history of Northeastern (Xiao et al., 2009).**

### 1.1.1.3 Broad Convergent Model

Sengor and Natalin (1996) suggested the Qilian Shan and the Qiadam oceanic and arc-type assemblages grew progressively southwestward by addition of accretionary complexes and magmatic arcs during the Late Proterozoic to Early Paleozoic (Figure 5). This model predicts inherited Early Paleozoic ages and similar U-Pb age distributions as adjacent regions, as well as possible Kunlun magmatic arc-related ages (Early Ordovician-Late Triassic) and Proterozoic strata with Archean age detrital-zircon grains shed from the Tarim basin and Alashan block to the north.

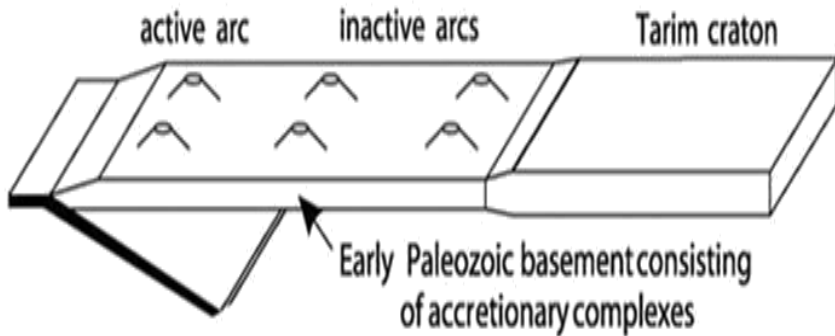


**Figure 5. Broad Convergent model (adopted from Gehrels et al., 2003).**

#### 1.1.1.4 The Northeast-facing Magmatic Arc Model

Sobel and Arnoud (1999) and Gehrels et al. (2003a, 2003b, 2011) interpreted the Qilian and the Qaidam terranes as a single crustal fragment formed by southwest-dipping subduction (Figure 6). Based on detrital zircon analyses, Gehrels et al. (2011) suggested that Proterozoic continental detritus from the Qilian Shan and the Qaidam terranes were not shed from the Tarim/Sino-Korean Craton, as they yield ages of 930-920 Ma and 820 Ma, which are not present in Proterozoic strata in Tarim and North China (which yield ages of 1.9 Ga-2 Ga). Moreover, similarities in zircon ages in the Qilian Shan and the Qaidam terranes were interpreted to indicate that the region was a single continental fragment during the mid-Proterozoic. During the Early Ordovician, subduction occurred along the northeastern and the southwestern margin of the composite Qilian Shan and Qaidam terranes. Furthermore, magmatism is interpreted to have migrated southward from the North Qilian to the Qaidam basin during the Ordovician to Early Silurian before final accretion to the Tarim and North China Cratons in the Early Silurian and Devonian. Devonian and younger platformal strata uncomfortably overlie all terrains and cratonal

regions (Gehrels et al., 2003).

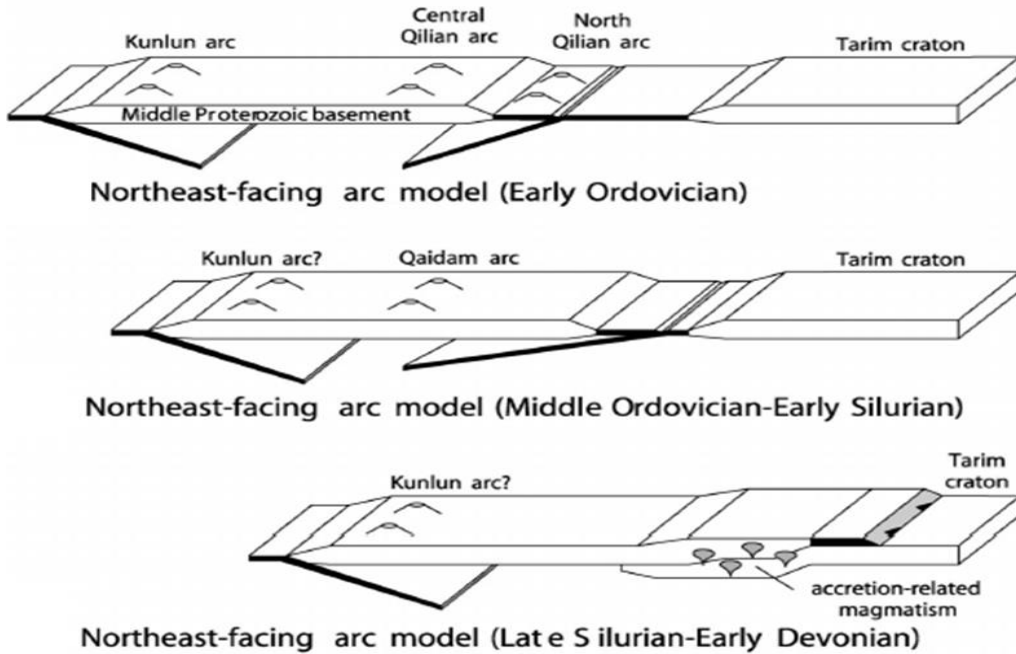


**Figure 6.** Neoproterozoic-Early Paleozoic tectonic evolution of Northeastern Tibet (Gehrels et al., 2011).

#### 1.1.1.5 Back-arc Convergent Model

Song et al. (2012) proposed a model which started with the opening of the Qilian Ocean at 710 Ma-520 Ma during breakup of the supercontinent Rodinia (Figure 7). Subsequently, the Qilian Ocean lithosphere was subducted northward beneath the Alashan block beginning at ~520 Ma which resulted in back-arc extension and opening of an ocean basin at 490 Ma. Both the Qilian ocean and back-arc basin were closed at ~440-420 Ma. This resulted in the collision with the Qilian-Qiadam block, which was subducted beneath the Alashan, resulting in UHPM of the northern end of the subducted block.

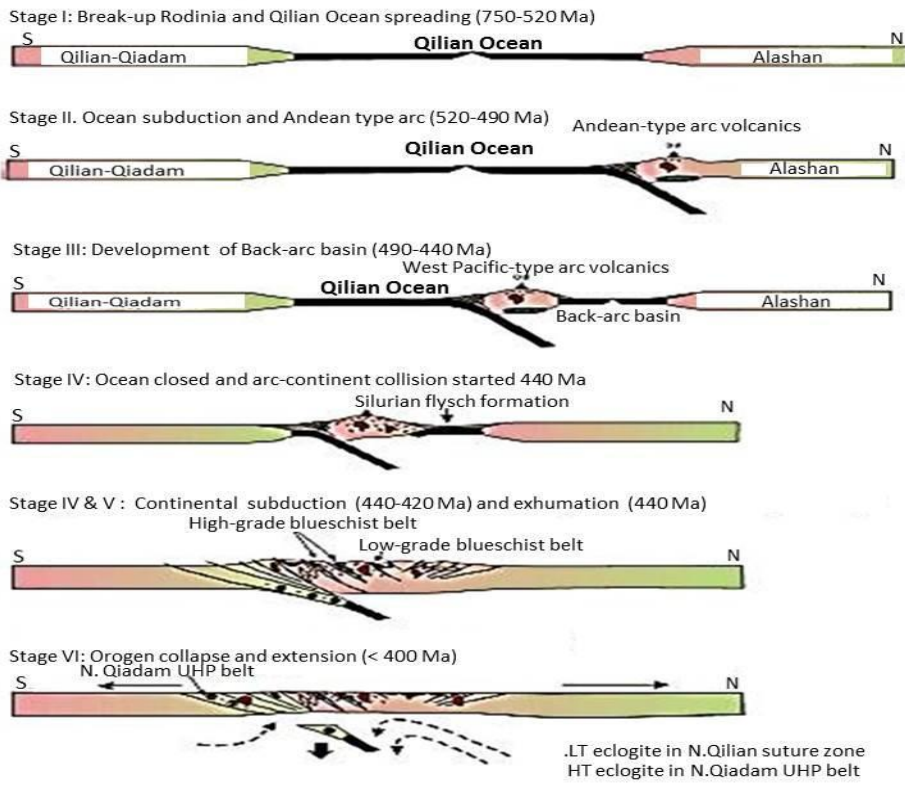


**Figure 7. Back-arc extension model during Late Proterozoic to Middle Paleozoic (Song et al., 2012).**

## 1.2 STRATIGRAPHY OF THE QING SHAN REGION

The Nan Shan region consists of mostly Middle Proterozoic to Early Paleozoic metasedimentary rocks, volcanic rocks, volcanic clast-rich strata, mélanges, shallow marine strata, and granitoid rocks (Gehrels et al., 2003).

Samples from sedimentary and metasedimentary units of a variety of ages were collected from the Qing Shan range along the southern margin of the Qilian Shan-Nan Shan Mountains (Figure 8). Previous geologic maps report ages of the sampled units to be from Precambrian basement units to Ordovician and Devonian sedimentary units. Two

samples were taken from metamorphic rocks interpreted to be Precambrian basement of the Nan Shan region (Figure 8A). Two samples were from Ordovician age strata, one of which is interpreted to be a metavolcanic unit, and another of which is a metasandstone. One sample was collected from a Devonian sandstone. The basal part of the Devonian sandstone consists of conglomerate, while the middle and upper parts are composed of gravel-bearing sandstone, siltstone, and sandstone with local intercalations of gypsum.

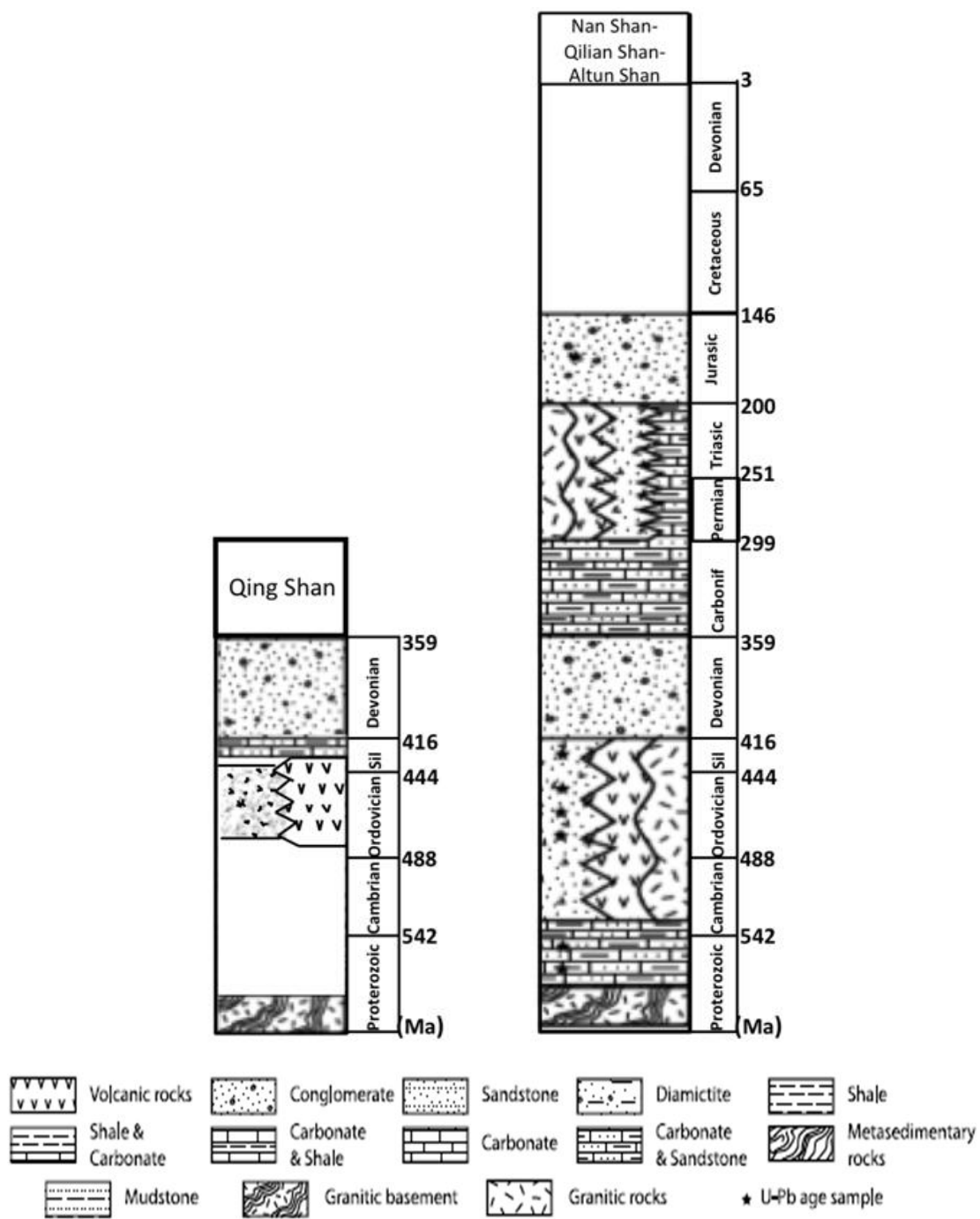


Figure 8. A) General stratigraphic column of the Qing Shan region B) General stratigraphic column of the Nan Shan, the Qilian Shan and the Altun Shan modified after Gehrels et al., (2011).

Sample 5-30-02-1 is from a biotite-hornblende bearing quartzite-metagraywacke. The sample is interpreted to be Proterozoic in age and comes from an outcrop extensively intruded by granitic bodies (Figure 9).



**Figure 9. Photograph showing Proterozoic metasandstone rocks intruded by granites.**

Sample 5-30-02-3A was collected from a biotite-muscovite quartz-rich metagraywacke (Figure 10) previously interpreted to be Proterozoic in age on regional geologic maps.



**Figure 10. Photograph showing Proterozoic metagraywackes.**

Sample 7-1-02-10 was collected from a metasandstone interpreted to be Ordovician in age which is in depositional contact with Ordovician (?) metavolcanics. This unit has preserved bedding which is overprinted by a pronounced foliation (Figure 11).



**Figure 11. Photograph showing Ordovician metasandstone.**

Sample 6-27-02-11 was collected from low grade metasandstone interpreted to be Paleozoic in age from an area dominated by metasandstone with minor layers of metavolcanic rocks. Metamorphic units show preserved bedding with a prominent superposed foliation (Figure 12).



**Figure 12. Photograph showing Paleozoic metasandstones.**

Sample 6-29-02-3 was collected from Devonian sandstone unit (Figure 13).

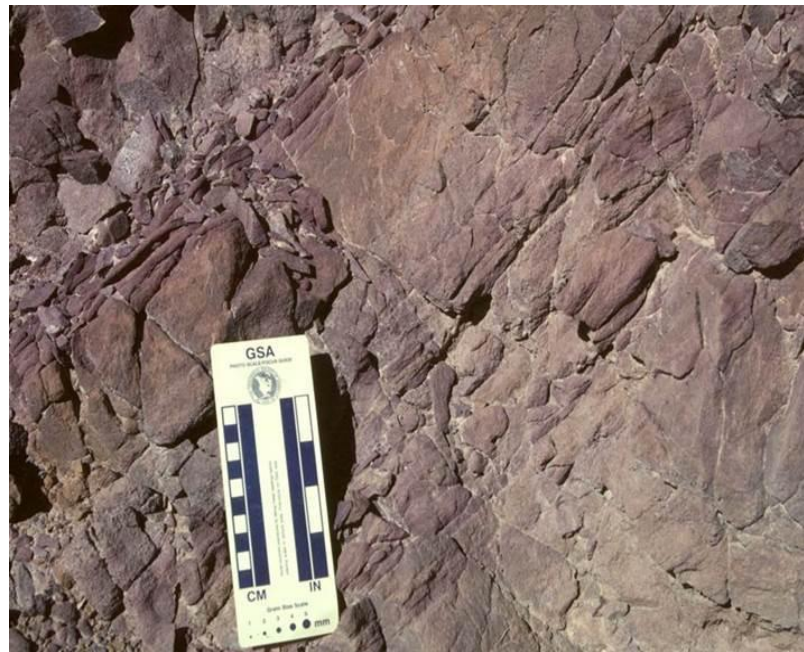


**Figure 13. Photograph showing Devonian sandstones.**

## CHAPTER 2

### 2. METHODS

#### 2.1.1 SAMPLE PREPARATION

Detrital zircons were separated from 1-3 kg samples of metasedimentary, metavolcanic, and sandstone units from the region (Figure 2). Rocks were crushed to <250 $\mu\text{m}$ . Zircons were then separated from the crushed samples using heavy liquids (methylene iodide, density of ~3.3 g/cm<sup>3</sup>) and magnetic separation. Zircon separates were then mounted in epoxy along with the standards Plesovice, Peixe, FC5z, and NIST glass. Grain mounts were then polished to expose the grains and photographed.

#### 2.1.2 ANALYTICAL METHODS

##### 2.2.1 Laser Ablation Inductively Coupled Mass Spectrometry (LA-ICPMS)

Zircon U-Th-Pb analyses were performed on a Varian quadrupole inductively coupled-mass spectrometer (Q-ICP-MS) at the University of Houston. Laser ablation was conducted using an Analyte 193 Ultra-Short Pulse Excimer laser ablation systems with a 25  $\mu\text{m}$  spot size. Sample delivery to the ICPMS was accomplished using helium as a carrier gas.

##### 2.2.2 Data Acquisition and Reduction

For each sample, data was obtained in 1-minute intervals. Background intensities were collected during the first 16 seconds followed by 20 seconds of laser ablation after which data continued to be collected for 24 seconds to allow the system return to background

values. Iolite v. 2.11 was used to import the signal intensities into Wavemetrics Igor ProTM (v. 6.2.0.0) software. Signal selection was made using Igor ProTM for all samples. A 16-second ablation time was selected to protect the data from contamination of initial  $^{204}\text{Pb}$  spikes during the first seconds of laser ablation. The selected signals were exported into an in-house Excel reduction spreadsheet. The baseline subtracted data included intensities for  $^{202}\text{Hg}$ ,  $^{204}\text{Hg}$ ,  $^{204}\text{Pb}$ ,  $^{206}\text{Pb}$ ,  $^{207}\text{Pb}$ ,  $^{208}\text{Pb}$ ,  $^{232}\text{Th}$ , and  $^{238}\text{U}$  with error uncertainties at the  $2\sigma$  level.

External standards were used to correct for instrumental drift by applying a fractionation factor of true ratio/measured ratio identified from the standard to the unknown measurements (Shaulis et al., 2010). Analytical accuracy of standards was identified by comparison of the mean values with mean standards weighted deviations (MSWD). Target standards were analyzed after every 5 unknown analyses. Auxiliary standards were analyzed after every 10 unknown analyses. Plesovice was used as a target standard for all samples (reported TIMS age of  $337 \pm 0.37$  Ma Slama, 2008). From target standard Plesovice, the mean values of auxiliary standard FC5z (reported ID-TIMS age of  $1096.2 \pm 1$  Ma Shaulis, 2010) was determined. Total combined mean values for three samples ( $1100.0 \pm 2.6$  Ma, MSWD = 0.80) is within  $< 1\%$  uncertainty of known standard age (Figure 14). Peixe (reported ID-TIMS ages of  $564 \pm 4$  Ma; Dickinson and Gehrels, 2003) was used as an auxiliary standard for two samples with the total combined mean value ( $575 \pm 12$  Ma, MSDW = 0.26) within  $< 3\%$  uncertainty of known standard age (Figure 14). To identify U and Th concentrations and make a correction for depth-dependent fractionation and bias, NIST 612 glass was analyzed three times at the end of the each analytical section (Pearce et al., 1997).

### 2.2.3 Isotope Systems

Detrital zircon analyses were conducted to interpret provenance linkages between various assemblages. For this purpose, ages were determined from zircon analysis, and the ages were correlated to the age of possible sources. Zircon ages were determined by analyzing the U/Pb ratio of individual zircon grains, particularly  $^{206}\text{Pb}/^{238}\text{U}$ ,  $^{207}\text{Pb}/^{235}\text{U}$ , and  $^{232}\text{Th}/^{208}\text{Pb}$ . These systems have relative values of uncertainties which vary as a function of age. The  $^{206}\text{Pb}/^{238}\text{U}$  age is more precise for ages younger than 1.5 Ga, while the  $^{206}\text{Pb}/^{207}\text{Pb}$  age is the least precise. For ages older than 1.5 Ga, the  $^{206}\text{Pb}/^{207}\text{Pb}$  age is more precise than  $^{206}\text{Pb}/^{238}\text{U}$  age, with the age resolution poorest around 1.4 Ga (Gehrels, 2008, 2010).

In addition to age information, U/Th ratios of the analyzed zircons can be used to assess the origin of the zircons. U/Th ratios of  $< 1$  can be interpreted to come from a mafic igneous source, while U/Th ratios of  $< 10$  are interpreted as coming from an igneous source in general, and U/Th ratios of  $> 10$  are interpreted to indicate metamorphic zircons (Gehrels et al., 2010). Furthermore, a 30% discordance cutoff was used for the study so that most Precambrian ages are retained.

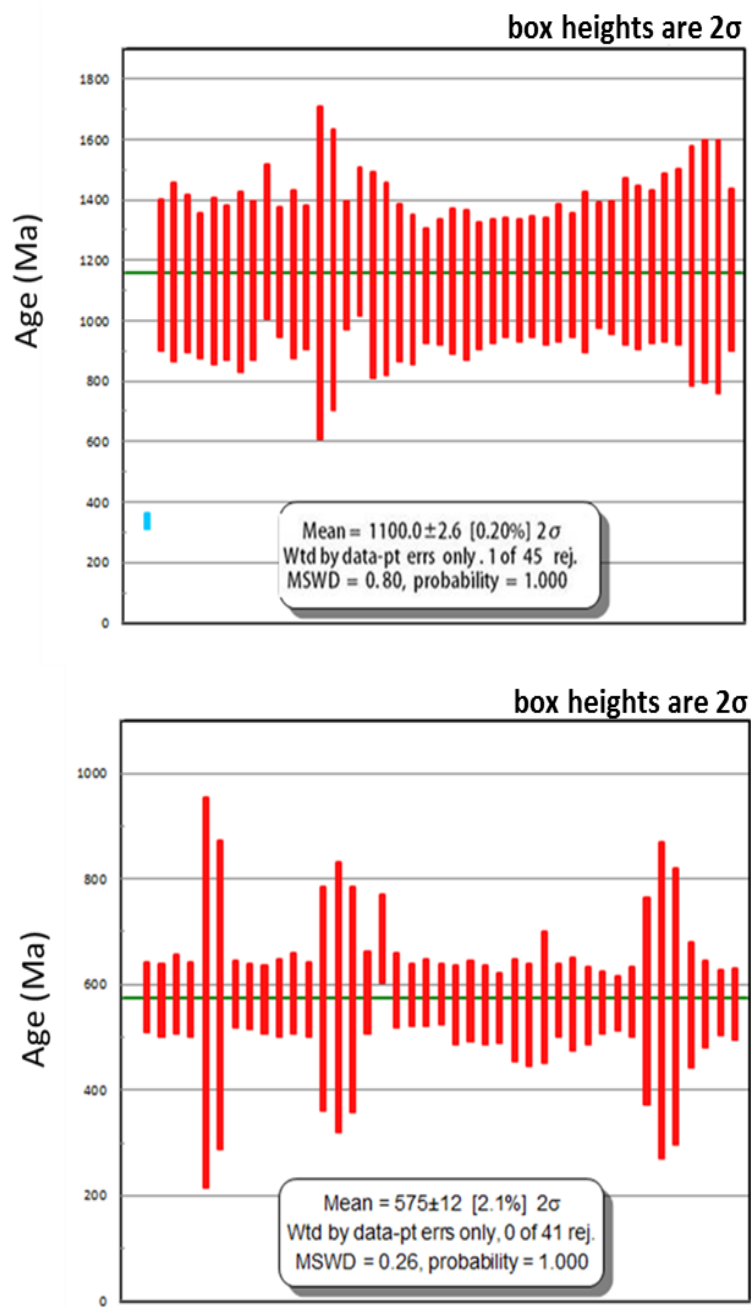


**Figure 14.** Mean value of FC5Z (top) and Peixe (bottom) standards with Mean Standard Weighted Deviations (MSWD) for combined values of sample sets for each unit. Errors are  $2\sigma$ .

## CHAPTER 3

### 3. RESULTS

#### 3.1 SAMPLE DATA

All ages are presented on Concordia plots, and Relative Probability Density Diagrams show ages that are < 30% discordant for each sample. Analytical results are presented in Auxiliary Data Tables A1-E1.

##### 3.1.1 5-30-02-1

65 zircon grains were analyzed from 5-30-02-1 of which 59 zircon grains yielded concordant ages (Figure 15 A and B, auxillary table A.1). The zircon grains from the sample generally are subrounded to rounded. The dated grains yielded ages between  $1583 \pm 26$  Ma to  $607 \pm 15$  Ma with defined age peaks at 734 Ma (7 grains), 779 Ma (6 grains), and 827 Ma (23 grains). The maximum depositional age for this sample is 734 Ma. This is age consistent with previous interpretations of the age of this unit. Interestingly, analyses indicate that all detrital zircon grains have a mafic origin with U/Th ratios less than 1 (Figure 16).

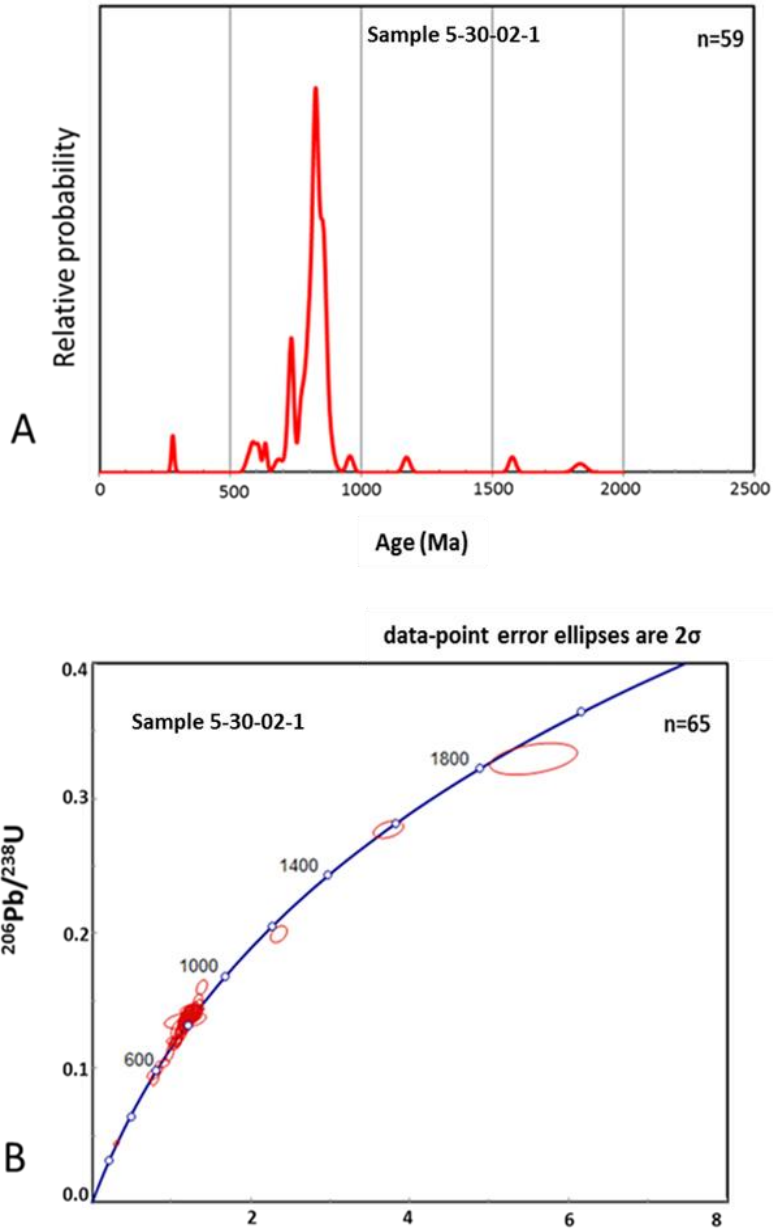


**Figure 15.** A) Relative age probability distribution plot of U-Pb ages determined for detrital zircon for sample 5-30-02-1, n= total number of grains analyzed. B) Pb/U Concordia diagram of sample 5-30-02-1. The clusters mainly concentrate around the 827 Ma peak age.

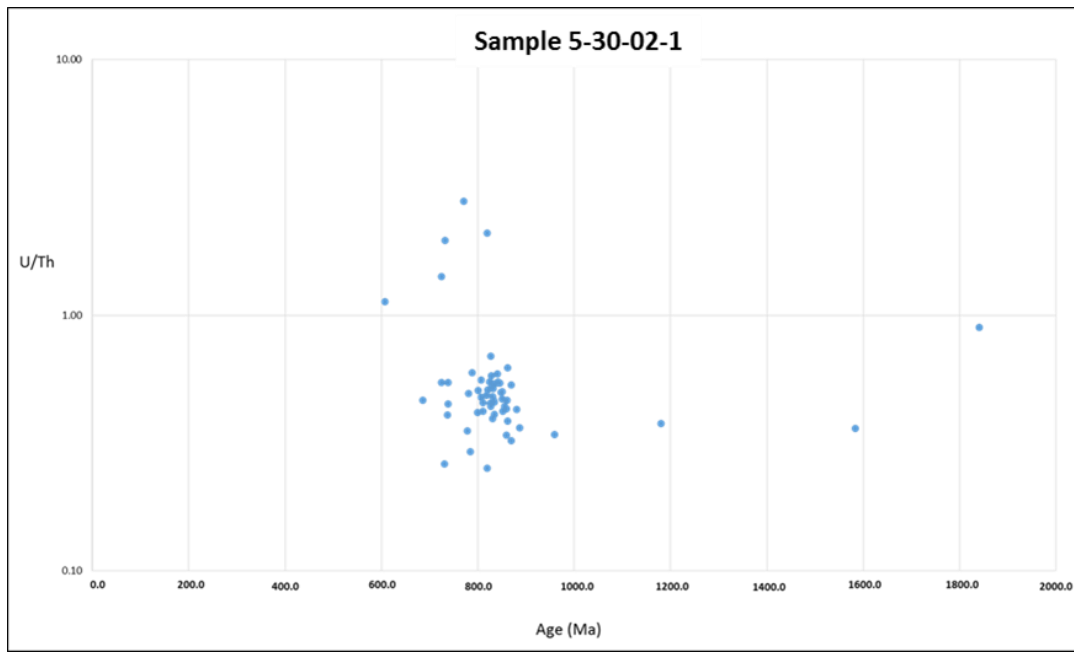


**Figure 16:**  $^{206}\text{Pb}/^{238}\text{U}$ -U/Th ratio of sample 5-30-02-1.

### 3.1.2 5-30-02-3A

Zircons from sample 5-30-02-3A are angular to subrounded. 103 grains were analyzed of which 46 yielded concordant results (Figure 17 A and B, auxillary table B.1). Age peaks are located at 434 Ma (11 grains), 459 Ma (4 grains), 527 Ma (4 grains), 982 Ma (4 grains), 1016 Ma (5 grains), and 1129 Ma (3 grains). Several other analyses are scattered between 1200 Ma and 2300 Ma. The sample yielded a Silurian maximum depositional age of 434 Ma. Nearly all analyses yielded U/Th ratios typical of igneous zircons (<10) (Figure 18).

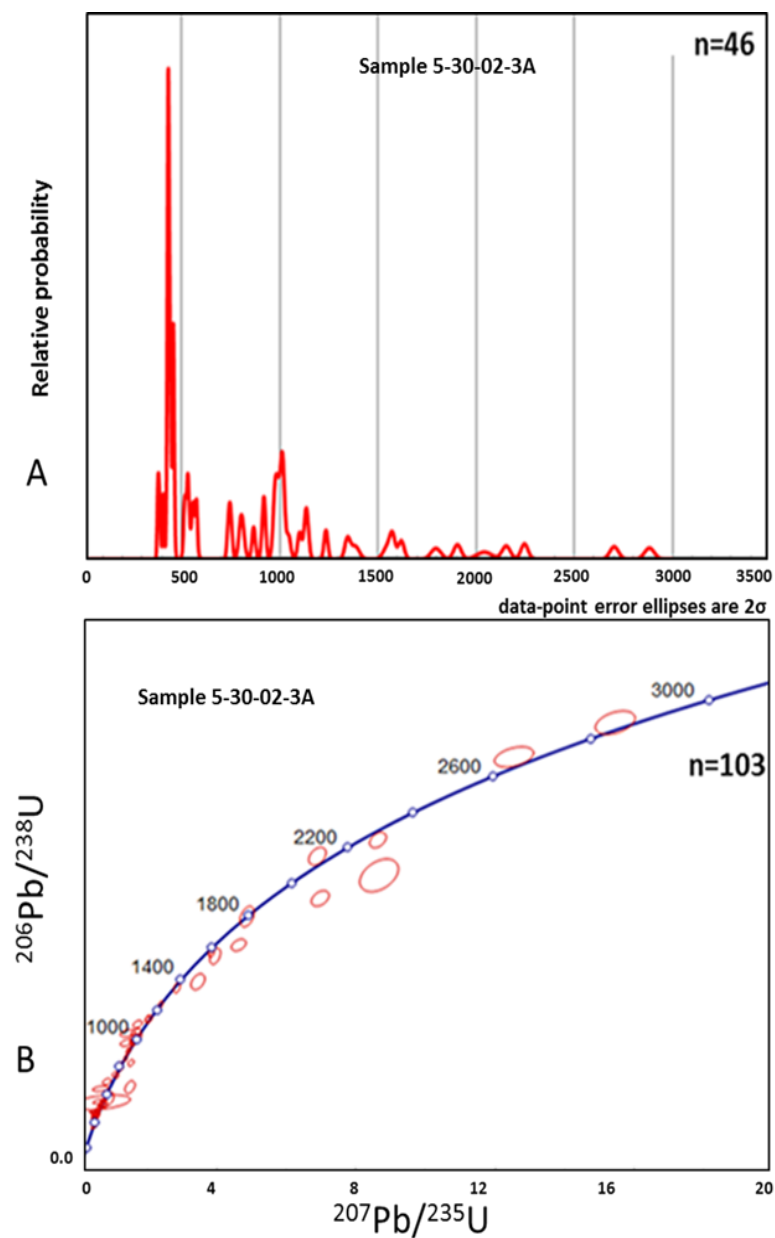


**Figure 17. A)** Relative age probability distribution plot of U-Pb ages determined for detrital zircon for sample 5-30-02-3A. **B)** Pb/U Concordia diagram of sample 5-30-02-3A.

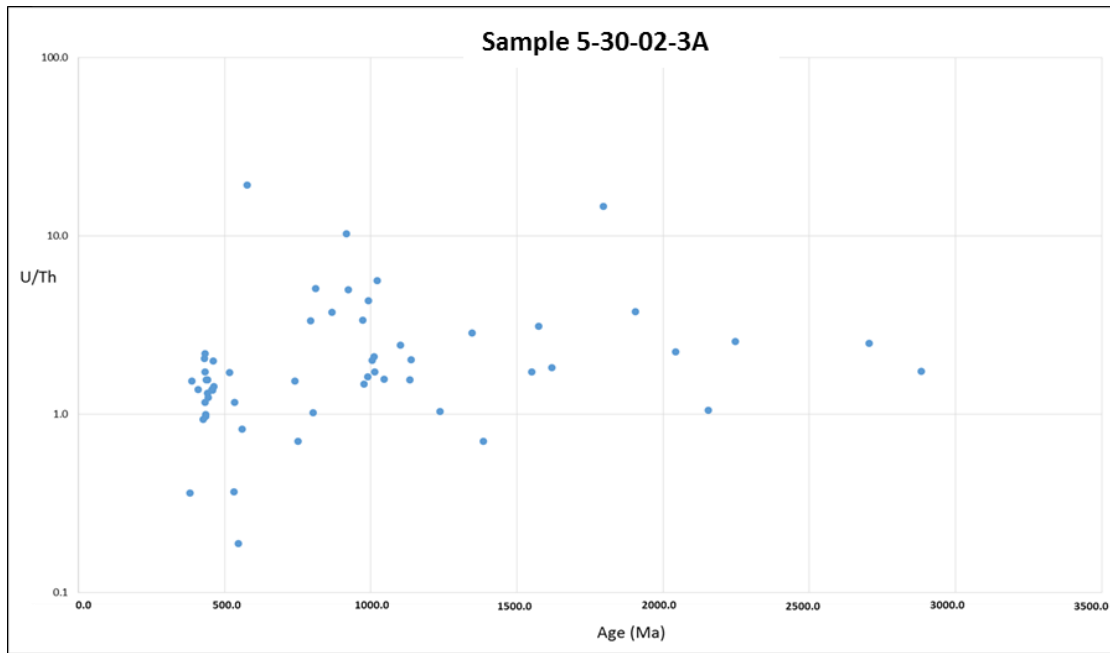


**Figure 18:**  $^{206}\text{Pb}/^{238}\text{U}$ -U/U/Th ratio of sample 5-30-02-3A

### 3.1.3 7-1-02-10

Zircons from sample 7-1-02-10 are angular to subrounded. 54 zircon grains were analyzed of which 16 yielded concordant results (Figure 19 A and B, auxillary table C 1). Ages range from 2720 Ma to 422 Ma with peak ages 460 Ma (4 grains), 2544 Ma (4 grains). The sample yields an Ordovician maximum depositional age of 460 Ma. All the concordant zircon grains are interpreted to be mafic origin due to  $\text{U}/\text{Th} < 1$  (Figure 20).

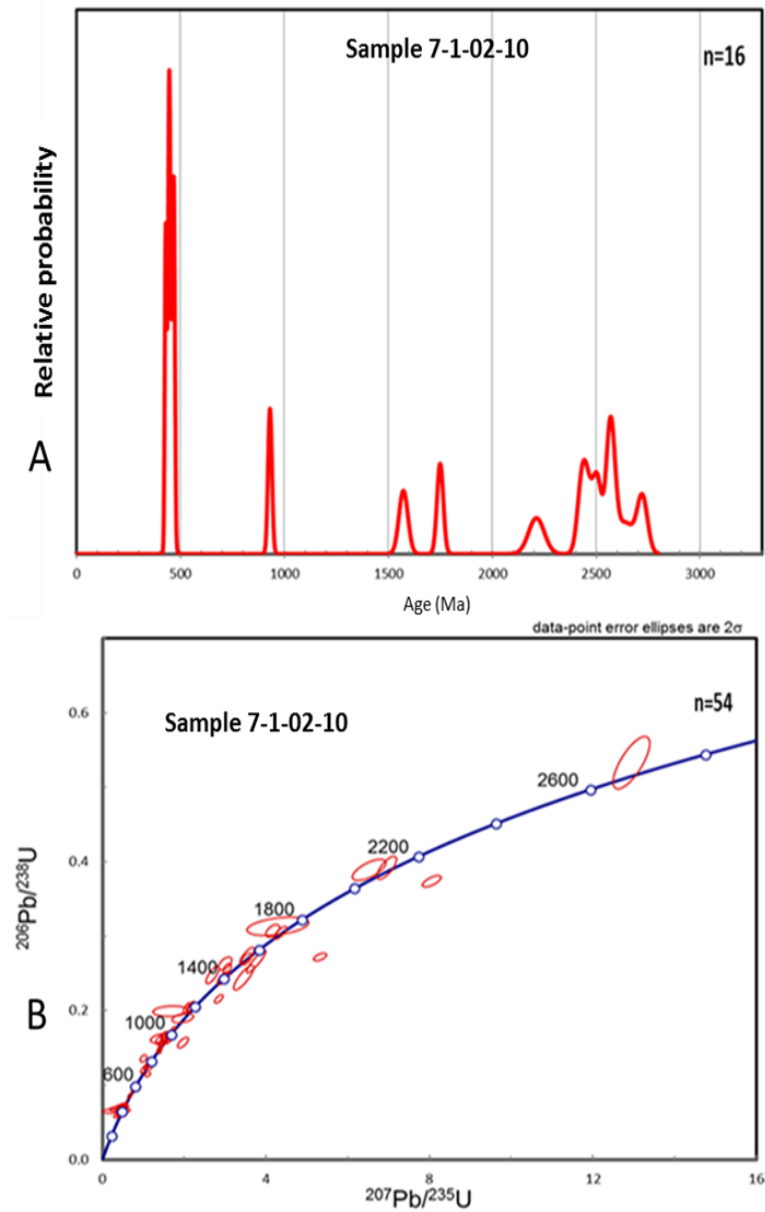


**Figure 19.** A) Relative age probability distribution plot of U-Pb ages determined for detrital zircon for sample 7-1-02-10. B) Pb/U Concordia diagram of sample 7-01-02-10.

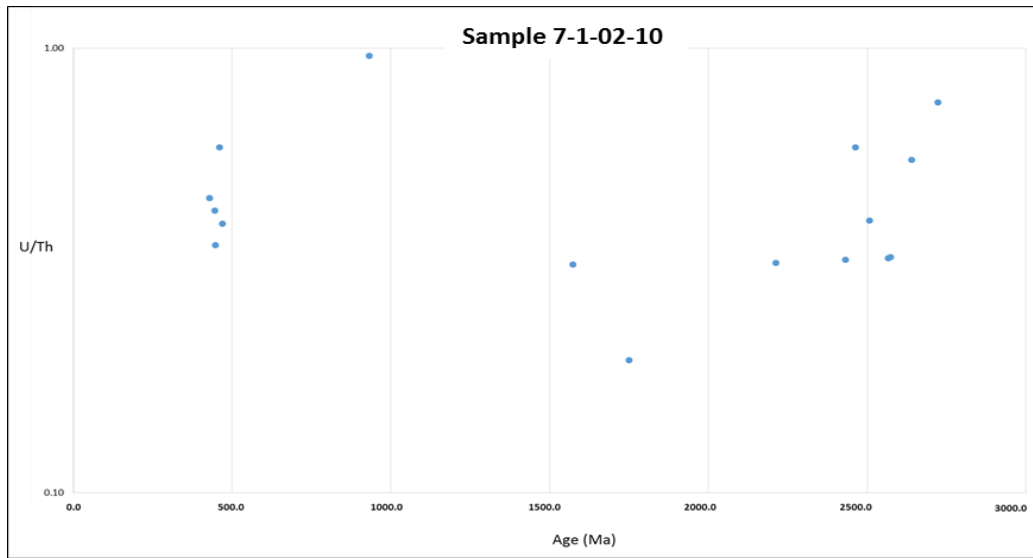


**Figure 20:**  $^{206}\text{Pb}/^{238}\text{U}$ -U/Th ratio of sample 7-01-02-10

### 3.1.4 6-27-02-11

Zircons from sample 6-27-02-11 are generally euhedral. 115 zircon grains were analyzed of which 23 yielded concordant ages (Figure 21 A and B, auxiliary table D.1). Ages range from 2198 Ma to 434 Ma with peak ages at 442 Ma (4 grains) and 1884 Ma (3 grains). Other analyses yielded ages scattered between 1000 Ma to 2300 Ma. The maximum age of deposition is 442 Ma. Zircon grains indicate mafic-igneous, igneous, and metamorphic origin (Figure 22).

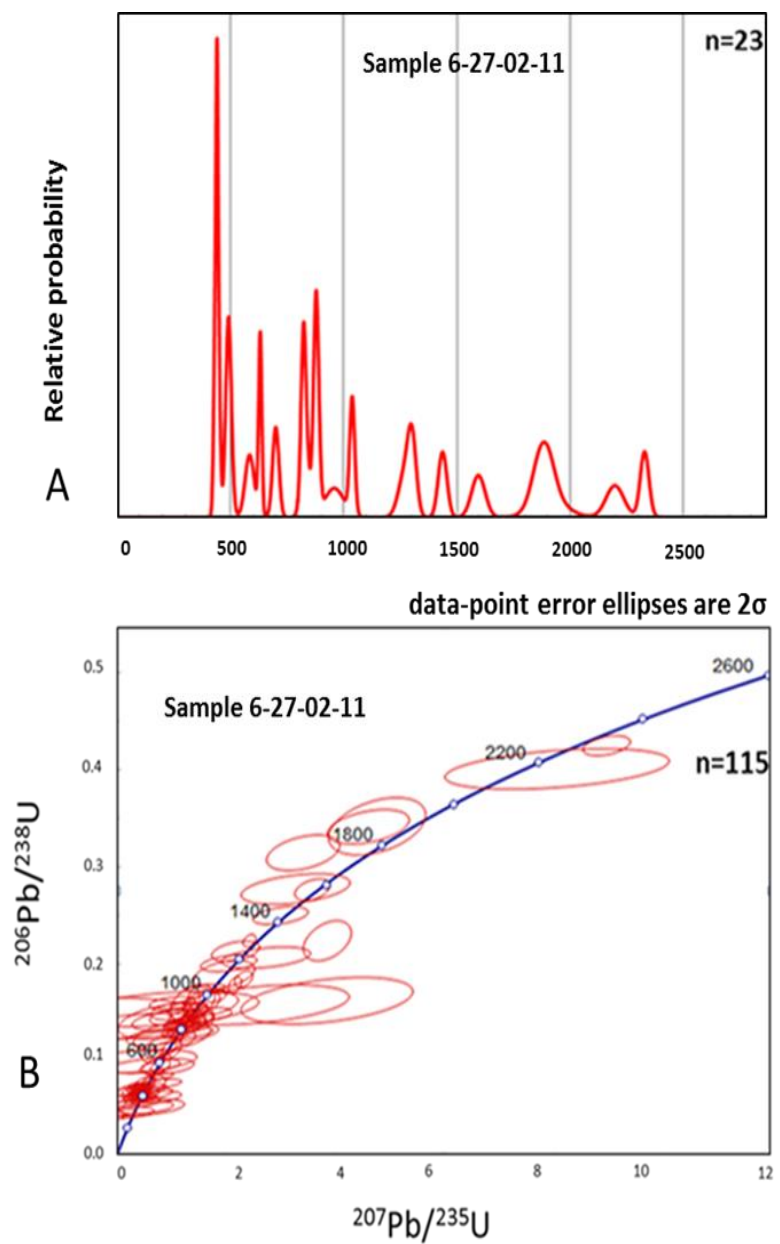


**Figure 21.** A) Relative age probability distribution plot of U-Pb ages determined for detrital zircon for sample 6-27-02-11. B) Pb/U Concordia diagram of sample 6-27-02-11

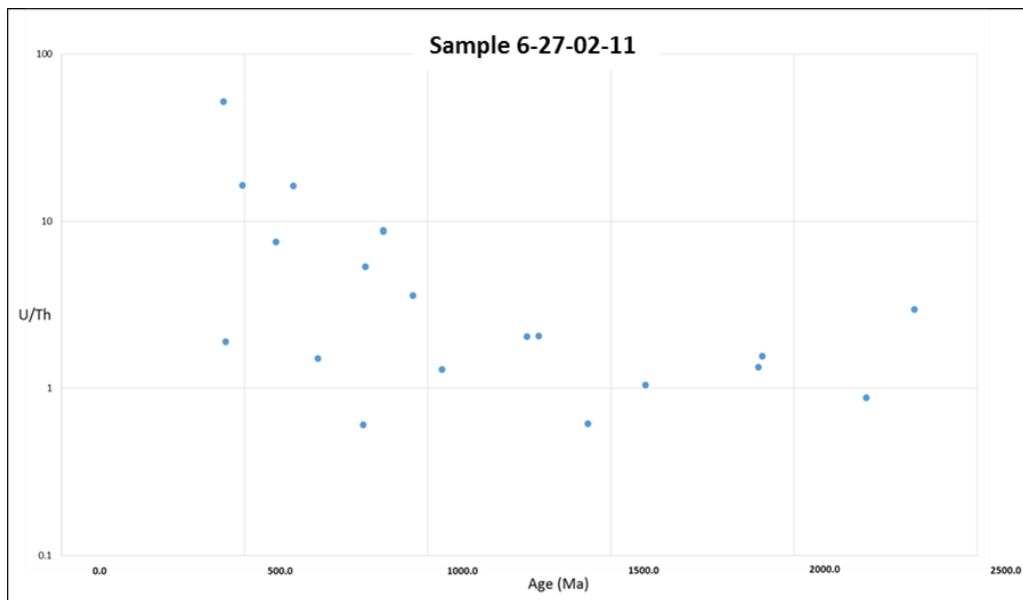


**Figure 22:**  $^{206}\text{Pb}/^{238}\text{U}$ -U/Th ratio of sample 6-27-02-11

### 3.1.5 6-29-07-3

Zircons from sample 6-29-07-3 are generally subrounded to rounded. 82 zircon grains were analyzed of which 19 yielded concordant ages (Figure 23 A and B, auxillary table E.1). The concordant ages range from  $3297 \pm 60$  Ma to  $436 \pm 33.2$  Ma. While the sampled lithology is interpreted to be Devonian in age, there are no Devonian detrital zircon grains and this sample does not have a well constrained maximum deposition age. However, the sample has a relatively strong age peak at 436 Ma (3 grains). Nearly all zircon grains indicate igneous origin (Figure 24).

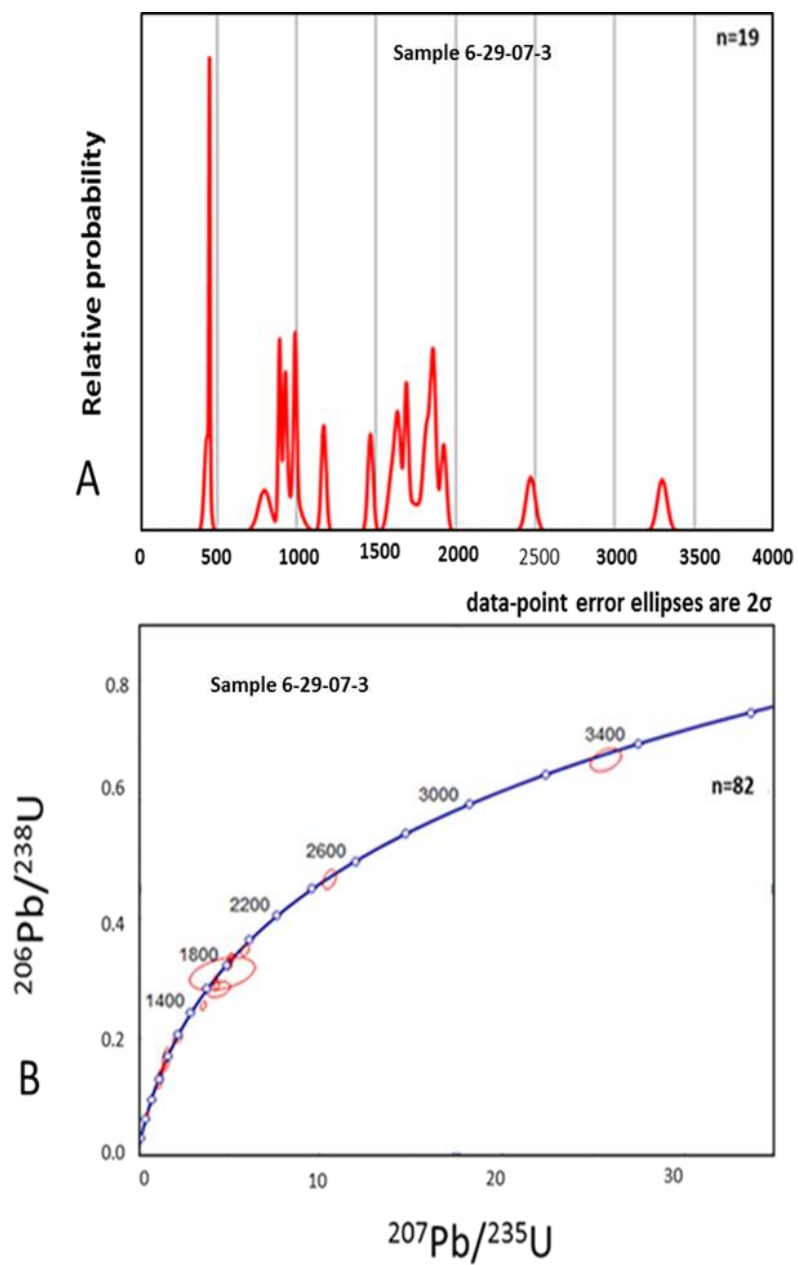


**Figure 23.** A) Relative age probability distribution plot of U-Pb ages determined for detrital zircon for sample 6-29-07-3. B) Pb/U Concordia diagram of sample 6-29-07-3.

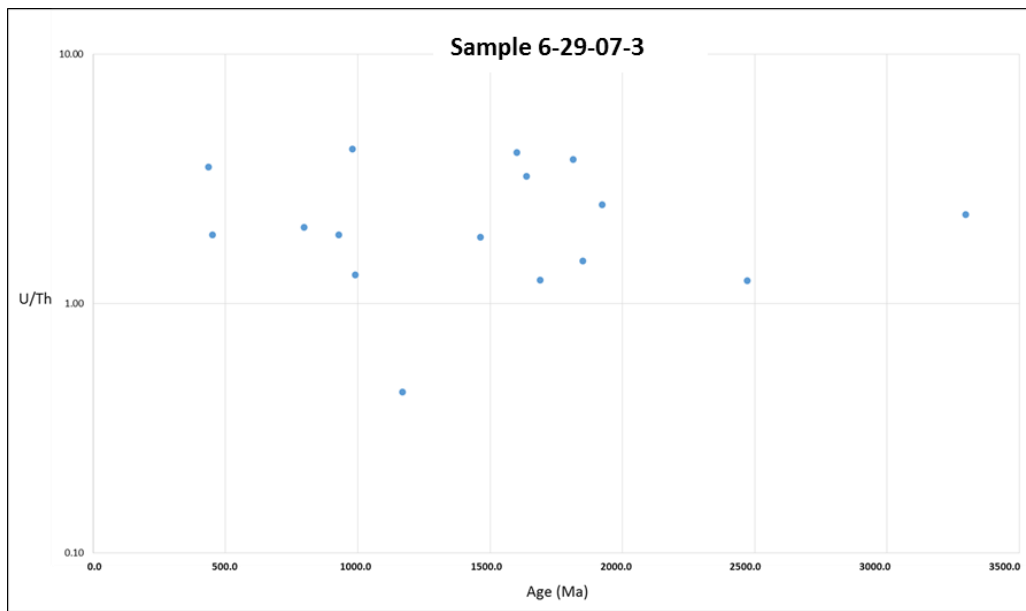


**Figure 24:**  $^{206}\text{Pb}/^{238}\text{U}$ -U/Th ratio of sample 6-29-07-3

## 3.2 DISCUSSION

### 3.2.1 POTENTIAL SOURCES

Analyzed samples yielded age peaks that can be grouped into identifiable age populations (Figure 25). Sample 5-30-02-1 is distinct from the other samples and yields a very different age signature in the Neoproterozoic. The sample has a limited detrital zircon age range with 827 Ma, 776 Ma and 734 Ma age peaks. Samples 5-30-02-3A, 7-01-02-10, 6-27-02-11 and 6-29-07-3 yielded similar Early Paleozoic age signatures between 400 Ma and 500 Ma. Furthermore, samples 5-30-02-3A, 6-27-02-11 and 6-29-07-3 yielded similar age signatures between 600 Ma and 1000 Ma as sample 5-30-02-1. However, the zircon grains in sample 5-30-02-1 are interpreted to have a mafic source due to  $U/Th < 1$  while zircon grains in all other samples generally indicate a non-mafic igneous or metamorphic origin with few exceptions.

For older age peaks, samples 7-01-02-10, 5-30-02-1, 5-30-02-3A and 6-27-02-11 have similar age signatures between 1500 Ma and 1850 Ma. Samples 7-01-02-10 and 6-29-07-3 have similar age signatures from 2200 Ma to 2700 Ma, although analyses from sample 7-01-02-10 in this age range indicate a mafic origin, while analyses from 6-29-07-3 have a non-mafic igneous origin. Sample 7-01-02-10 has the strongest Archean signature with a prominent peak at ~2500 Ma.

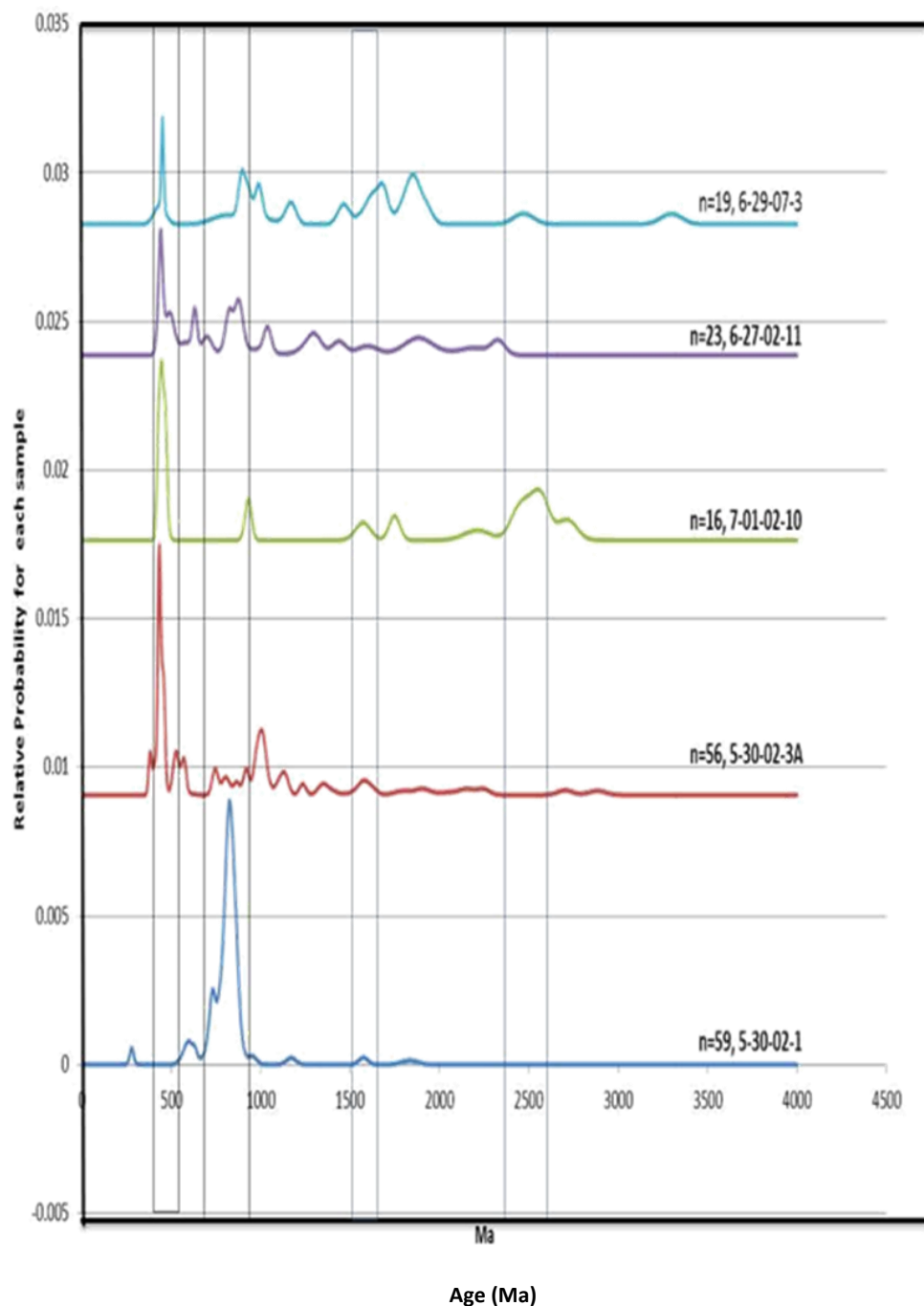


**Figure 25.** Relative age probability distribution plot of U-Pb ages determined for detrital zircon of all samples.

### 3.2.2. 5-30-02-1

Proterozoic sample 5-30-02-1, which is depicted as part of the regional basement on regional geologic maps, lacks detrital zircon grains of Archean age, with only two Mesoproterozoic grains ( $1181\pm27$  Ma,  $1583\pm26$  Ma). Instead, the sample contains 827 Ma (23 grains), 779 Ma (6 grains) peaks ages with a 774 Ma (7 grains) maximum depositional age (Figure 17). While this sample may represent the regional basement, 820 Ma zircons have been recognized in Danjin Shan metasedimentary unit and are interpreted to be derived from Australia, North China, and South China (Gehrels et al., 2003) (Figure 1). Another possibility is that the Neoproterozoic zircons were shed from local igneous sources. An important aspect to note is that nearly all the grains yielded U/Th ratios indicating a mafic origin (Figure 16).

### 3.2.3. 5-30-02-3A

Sample 5-30-02-3A has previously been interpreted to be Proterozoic metagraywacke based on regional geologic maps (Figure 26). However, zircon data shows it to be significantly younger, with a Late Ordovician–Early Silurian maximum depositional age of 434 Ma (11 grains) (Figure 17). Most of the zircon grains were likely derived from contemporaneous magmatic sources due to  $U/Th < 10$  (Figure 18). The unit has two Proterozoic age peaks at 1016 Ma (5 grains) and 1129 Ma (3 grains). A possible source for the older zircon grains is the nearby Yema Shan volcanic clast-rich feldspathic wacke which has zircon ages between 1.2–1.0 Ga (Gehrels et al., 2003) (Figure 1). The sample also yields 527 Ma (4 grains) and 459 Ma (4 grains) age peak ages. Zircon ages between 740 Ma to 860 Ma likely come from the regional basement.



**Figure 26:** Geologic map over Google Earth image showing sample 5-30-2-3A location. (GTOPO30,12.01.1996).

### 3.2.4 7-01-02-10

Sample 7-1-02 contains an Archean age peak 2544 Ma (4 grains) with a 460 Ma maximum depositional age (4 grains) (Figure 19). A possible source for older grains could be nearby of Dangin Shan quartose metaturbidites; also these zircons might come from North China Craton. The younger age peak is attributed to a mafic igneous source due to U/Th ratio less than 1 (Figure 20).

### 3.2.5 6-27-02-11

Sample 6-27-02-11 contains age peaks at 442 Ma (4 grains) and 1884 Ma (3 grains) (Figure 21). An interesting observation is that all the grains which make up the 442 Ma

age peak have a metamorphic origin. One possibility is that these were sourced from the Qiadam Ultra High Pressure Metamorphic belt. The other grains are igneous origin due to U/Th ratio less than 10 (Figure 22).

### 3.2.6 6-29-07-3

Sample 6-29-07-3 includes one  $436 \pm 33$  zircon grain, and other grains which scatter from 800 Ma to 1800 Ma, all of which are igneous in origin (U/Th less than 10). This sample does not have a well constrained maximum depositional age. However, the sample has a relatively strong age peak at 436 Ma (3 grains). The older inherited zircon grains may have been shed from the North China Craton or the regional basement. Nearly all the zircon grains have U/Th ratios which indicate an igneous origin (Figure 24).

## 3.3 TECTONIC MODELS

The analyzed data from sample 5-30-02-1 document a very significant Precambrian age signature. The sedimentary basement rock yields 827 Ma and 779 Ma peak ages with a 734 Ma maximum depositional age, and all grains indicated a mafic source. While this sample might represent the regional basement, another possibility is that the zircons were shed from local igneous sources related to the rifting of continental crust due to the mafic U/Th signature. With the exception of sample 5-30-02-1, all the samples yielded Early Paleozoic (Ordovician to Silurian) maximum depositional ages, and broadly similar age distributions.

My data are inconsistent with the Broad convergent model. The model suggests that the

basement beneath the Nan Shan and Qilian Shan is composed of Early Paleozoic units, whereas my data show the presence of basement as old as late Proterozoic. Also, this model suggests that the strata deposited during the Early Paleozoic should be sourced from oceanic arc settings. The data from my study do not support this interpretation due to the presence of strong older inherited component that could not be derived from a series of island arc terranes. Further, this model suggests that Proterozoic continental detritus in the Nan Shan were shed from the Archean age Alashan block, whereas Proterozoic sample 5-30-02-1 did not reveal any Archean age detrital zircon signatures (Figure 5).

The Archipelago and the Multiple-accretionary models predict similar tectonic evolutions of the region (Figures 3, 4). These models suggest that the basement of the Nan Shan region is as old as late Proterozoic (Xia et al., 1996). The Archipelago and the Multiple-accretionary models suggest that the volcanic arcs were built on older continental crust explaining the older inherited zircon grains. Furthermore, an ocean basin between the Qaidam and the Nan Shan terranes is interpreted to have been subducted during the Late Cambrian to Early Silurian beneath the Nan Shan, and may have resulted in magmatism related to the observed Early Paleozoic zircon grains. The presence of the high pressure metamorphic rocks in Nan Shan region suggests a suture zone between Nan Shan and Central Qilian Shan, which is consistent with these models.

The North-facing Magmatic Arc model interprets that the basement beneath the Nan Shan region consists of mid-Proterozoic units (Gehrel et al., 2003), whereas the data indicate a basement age as old as late Proterozoic (Figure 6). The model suggests similar age signatures during the Early Paleozoic, as documented in this study (Figure 27). Granitoid ages from the region are between 482 Ma and 459 Ma, which are consistent with

peak ages in the detrital record (Figure 28). According to Gehrels et al. (2003), these ages are interpreted to be related to the North Qilian Ocean subduction southward beneath the Qilian Shan. Southward subduction of the North Qilian Ocean may have resulted in magmatism related to the Early Paleozoic zircon grains. However, the suture zone between the Central Qilian Shan and the Nan Shan does not exist according to this model.

Proterozoic sample 5-30-02-1 yielded all mafic origin zircon grains that might be explained by rifting of continental crust. This interpretation is consistent with the Back-arc extension model, which suggests that Rodinia breakup started during the Neoproterozoic and triggered the opening of the Qilian Shan Ocean (Figure 7). Furthermore, Early Paleozoic strata in the Qing Shan contain Archean age detrital zircons that might have been shed from the rifted continental fragment.

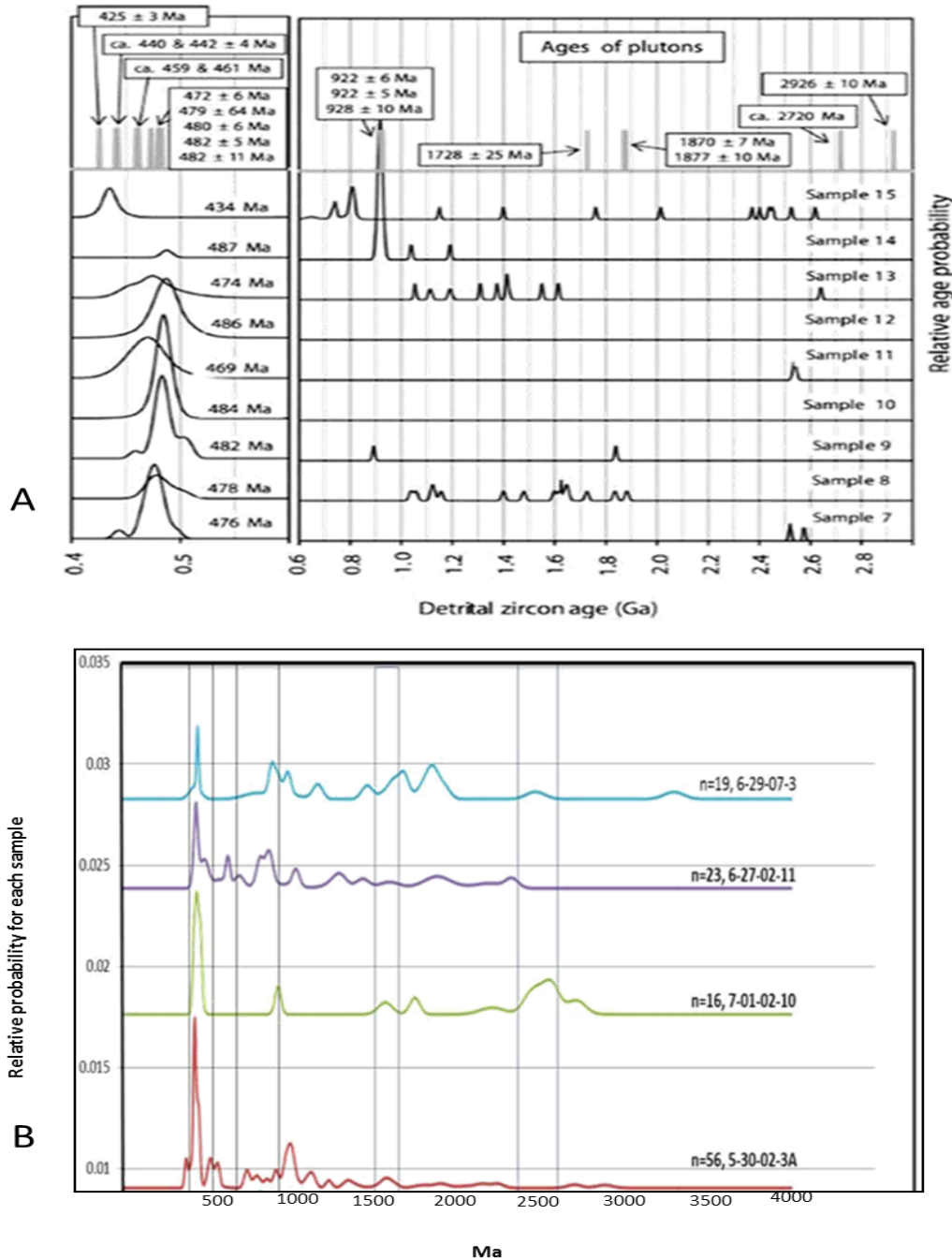
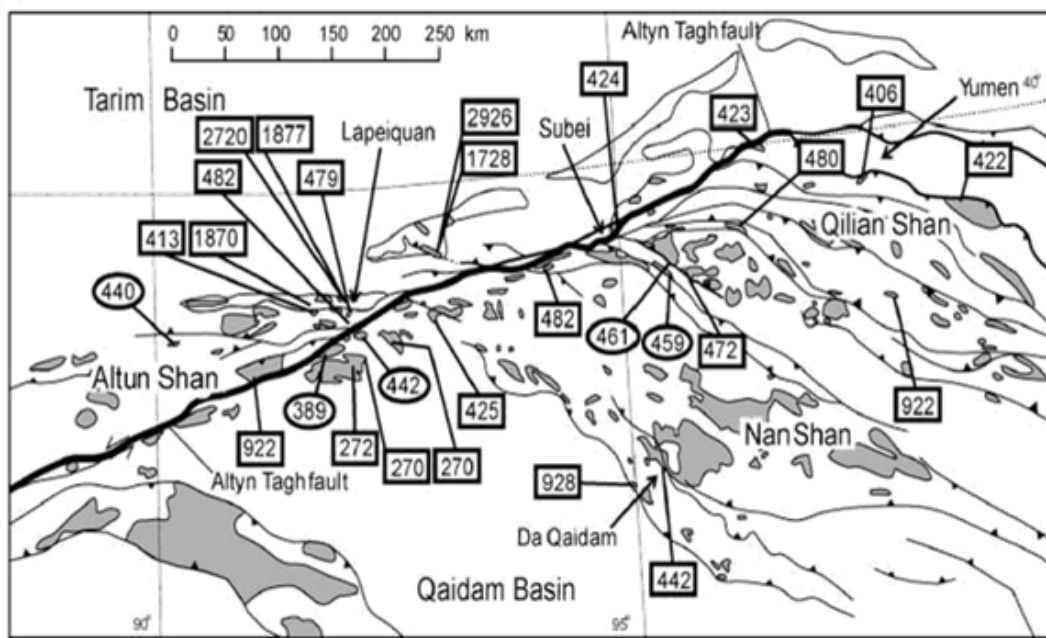


Figure 27. A) Relative age probability diagram comparing ages of detrital-zircon grains from samples of magmatic arc affinity and recycled orogenic provenance (black curves) (from Gehrels et al., 2003). Peak age probabilities are shown for the younger grains. Also shown in gray bars are Pb/U ages of plutonic rocks from the region from Gehrels et al., (2003) and Cowgill et al., (2003). B) Relative age probability distribution plots of U-Pb ages determined from detrital zircons from four samples.



**Figure 28.** Map showing available U-Pb ages of plutonic rocks in the study area (Gehrels et al. (2003) and Cowgill et al., (2003)).

## CHAPTER 4

### 4. CONCLUSION

I conducted detrital zircon U/Pb geochronologic analyses on five samples from Proterozoic metasediments and Early Paleozoic sandstones, which yielded 173 concordant zircon analyses. Proterozoic sample 5-30-02-1, interpreted to represent the regional basement, yields a strong 827 Ma age peak with a 734 Ma maximum depositional age. Although a nearby sample (5-30-02-3A) is also from lithologies previously interpreted to be Proterozoic in age, my results show that the sample is Early Paleozoic in age with a Silurian maximum depositional age of 434 Ma. All other samples yielded Early Paleozoic (Ordovician to Silurian) maximum depositional ages, and broadly similar age distributions.

Sample 5-30-02-1 has a distinct Neoproterozoic age distribution, with all analyses yielding U/Th ratios typical of mafic zircons. While these zircon grains could have been derived from the Australia, North China, or South China Cratons, another more likely interpretation is that they are a result of Neoproterozoic continental rifting (Figure 7).

All other samples yield Early Paleozoic maximum depositional ages with broadly similar age distributions. Early Paleozoic (Ordovician through Silurian) ages could either reflect; 1) southward subduction of the North Qilian terrane beneath the Qilian Shan, or 2) northward subduction of an ocean basin north of the Qiadam terrane beneath the Nan Shan terrane during the Late Cambrian to Early Silurian resulting in magmatism related to the observed Early Paleozoic ages. Finally, the sample from the Devonian unit does not yield any ages younger than Silurian, consistent with the interpretation that Devonian strata postdates the accretion of Qilian Shan and the Qiadam terranes to the North China Craton and related igneous activity.

## **REFERENCES CITED**

- Bureau of Geology and Mineral Resources of Ningxia Province (1990). Regional Geology of Ningxia Province. Geological Memoirs of Ministry of Geology and Mineral Resources of People's Republic of China: Geological Publishing House, v. 217, no. 22, p. 516-517.
- Cowgill, E., Yin, A., Harrison, TM., and Wang, X.-F., 2003, Reconstruction of the Altyn Tagh fault based on U-Pb geochronology: The role of backthrusts, mantle sutures, and heterogeneous crustal strength in forming the Tibetan plateau: *Journal of Geophysical Research*, v.180, no. B7, p. 2346, doi:10.1029/2002JB002080.
- Dickinson, W.R., and Gehrels, G.E., 2003; U-Pb ages of detrital zircons from Permian and Jurassic eolianite sandstones of the Colorado Plateau, USA: Paleogeographic implications: *Sedimentary Geology*, v. 163, p. 29-66.
- Gehrels, G.E., Yin, A., and Wang, X.-F., (2003a). Detrital zircon geochronology of the northeastern Tibetan Plateau, *Geol. Soc. Am. Bull.*, v. 115, p. 881-896.
- Gehrels, G. E., and A. Yin (2003b), Magmatic history of the northeastern Tibetan Plateau, *J. Geophys. Res.*, v. 108, no. B9, p. 2324, doi:10.1029/2002JB001876.
- Gehrels, G. E., Valencia, V. A., and Ruiz, J., 2008, Enhanced precision, accuracy, efficiency, and spatial resolution of U-Pb ages by laser ablation-multicollector inductively coupled plasma- mass spectrometry. *Geochemistry, Geophysics, Geosystems*, v, 9, p.1-13.
- Gehrels, G., 2010; Detrital zircon U-Pb geochronology: Current methods and new opportunities, in: Recent Advances in Tectonics of Sedimentary Basins, C. Busby and A. Azor, editors, Blackwell Publishing.
- Gehrels, G., Kapp, P., DeCelles, P., Pullen, A., Blakey, R., Weislogel, A., Ding, L., Guynn, J., Martin, A., McQuarrie, N., Yin, A., 2011. Detrital zircon geochronology of pre-Tertiary strata in the Tibetan-Himalayan orogen. *Tectonics*, v. 30, no. 5, p. TC5016.
- Geng, Y.-S., Wang, X.S., Shen, Q.H., Wu, C.M., 2007. Chronology of the Precambrian metamorphic series the Alxa area, Inner Mongolia. *Journal of Asian Earth Sciences*, v. 34, p. 251–261.

Hsu, K.J., Guitang, P., and Sengor, A.M.C., 1995, Tectonic evolution of the Tibetan plateau: A working hypothesis based on the archipelago model of orogenesis: International Geology Review, v. 37, p. 473-508.

Li, C.Y., Liu, Y., Zhu, B.C., Feng, Y.M., and Wu, H.C., 1978, Structural evolution of Qinling and Qilian Shan, in Scientific papers in Geology and International Exchange: Beijing, Geologic Publishing House, p. 174-197.

Liu, Z.Q., 1988, Geologic map of the Qinghai-Xizang (Tibetan) plateau and adjacent areas: Beijing, Geological Publishing House, Chengdu Institute of Geology and Mineral Resources, scale 1:1,500,000.

Pearce, N.J.G., Perkins, T.W., Westgate, J.A., Gorton, M.P., Jackson, S.E., Neal, C.R., and Chinery, S.P., 1997; A compilation of new and published major and trace element data for NIST SRM 610 and NIST SRM glass reference materials. Geostandards Newsletter, Journal of Geostandards and Geoanalysis, v. 21, p. 115-144.

Sengor, A.M.C., and Natalin, B.A., 1996, Paleotectonics of Asia: Fragments of a synthesis, in Yin, A., and Harrison, T.M., eds., The Tectonics of Asia: New York, Cambridge University Press, p. 486-640.

Shaulis, B., Lapen, T.J., and Toms, A., 2010; Signal linearity of an extended range pulse counting detector. Applications to accurate and precise U-Pb dating of zircon by laser ablation quadrupole ICP-MS. Geochemistry, Geophysics, Geosystems, v. 11, Q0AA11, doi:10.1029/2010GC003198. issn: 1525-2027.

Slama, J., Dunkley, D.L., Kachlik, V., and Kusiak, M.A., 2008; Transition from island arctic passive setting on the continental margin of Gondwana: U-Pb zircon dating of Neoproterozoic metaconglomerates from the SE margin of the Tepla Barrandian Unit, Bohemian Massif. Tectonophysics, v. 461, p. 44-59.

Sobel, E.R., Arnaud, N., 1999. A possible middle Paleozoic suture in the Altyn Tagh, NW China. Tectonics, v. 18, no. 1, p. 64–74.

Song, S.G., Su, L., Li, X.H., Niu, Y.L., Zhang, L.F., 2012. Grenville-age orogenesis in the Qaidam-Qilian block: the link between South China and Tarim. Precambrian Research, v. 220–221, p. 9–22.

Song, S. G.; Niu, Y. L.; Su, L., 2013. Tectonics of the North Qilian orogen, NW China. Gondwana Research, v. 23, p. 1378-1401, doi: 10.1016/j.gr.2012.02.004.

Tung, K.A., Yang, H.J., Yang, H.Y., Liu, D.Y., Zhang, J.X., Wan, Y.S., Tseng, C.Y., 2007b. SHRIMP U-Pb geochronology of the zircons from the Precambrian basement of the Qilian Block and its geological significances. *Chinese Science Bulletin*, v 52, p. 2687–2701.

Xia, L., Xia, Z., and Xu, X., 1996, Origin of the oceanic island arc system in the northern Qilian Shan: Beijing, Geological Publishing House, 153 p.

Xiao, W.J., Windley, B.F., Yong, Y., Yan, Z., Yuan, C., Liu, C.Z., Li, J.L., 2009. Early Paleozoic to Devonian multiple-accretionary model for the Qilian Shan, NW China. *Journal of Asian Earth Sciences*, v. 35, p. 323-333.

Xiong, J., and P. J. Coney, Accreted terranes of China, in Tectonostratigraphic Terranes of the Circum-Pacific Region, *Earth Sci. Ser.*, vol. 1, edited by D. G. Howell, p. 349–361, Circum-Pac. Counc. for Energy and Miner. Resour. Houston, Tex., 1985.

Xiu, Q.Y., Yu, H.F., Li, Q., Zuo, G.C., Li, J.W., Cao, C.J., 2004. Discussion on the petrogenetic time of Longshoushan Group, Gansu Province. *Acta Geologica Sinica*, v. 78, p. 366–373.

Yin, A., and Harrison, T.M., 2000, Geologic evolution of the Himalayan-Tibetan orogen: *Annual Review of Earth and Planetary Sciences*, v. 28, p. 211-280

## APPENDIX A- Zircon Data Tables

**Table A.1: 5-30-02-1**

45

Cone.	(ppm)						Ratios						Ages				
	Spot	[U]	[Th]	U/Th	$^{206}\text{Pb} / ^{238}\text{U}$	$2\sigma$	$^{207}\text{Pb} / ^{235}\text{U}$	$2\sigma$	$^{207}\text{Pb} / ^{230}\text{Pb}$	$2\sigma$	$^{206}\text{Pb} / ^{238}\text{U}$	$2\sigma$	$^{206}\text{Pb} / ^{238}\text{U}$	$2\sigma$	$^{206}\text{Pb} / ^{238}\text{U}$	$2\sigma$	%Disc
	1	145.9	245.7	0.6	0.09536	3.372	0.775101	8.077	0.058951	7.17	587.2	18.9	582.69	35.8	565	156	-3.7
	2	271.9	719.6	0.4	0.199372	2.522	2.352166	3.641	0.085566	2.103	1171.9	27	1228.21	25.9	1328	41	13.4
	3	146.3	348.3	0.4	0.133825	2.720	1.190774	3.711	0.064534	2.334	809.7	20.7	796.32	20.5	759	49	-6.2
	4	170.0	312.0	0.5	0.118720	2.722	1.015443	3.370	0.062034	2.196	723.2	18.6	711.62	17.2	675	47	-6.6
	5	175.4	398.6	0.4	0.136573	2.786	1.210304	3.665	0.064273	2.613	825.3	21.6	805.33	20.4	751	55	-9.0
	6	128.5	269.3	0.5	0.132778	2.585	1.190055	3.747	0.065004	2.918	803.7	19.5	795.99	20.7	774	61	-3.6
	7	197.3	139.4	1.4	0.118477	3.437	1.049608	5.451	0.064253	4.365	721.8	23.5	728.69	28.4	750	92	3.9
	8	221.8	371.3	0.6	0.129757	2.627	1.148288	3.229	0.064183	2.164	786.5	19.5	776.43	17.5	748	46	-4.9
	9	160.8	248.8	0.6	0.103070	2.345	0.884347	8.214	0.062228	7.945	632.4	14.1	643.33	39.2	682	170	7.8
	10	70.0	278.3	0.3	0.135104	2.182	1.158656	3.292	0.062199	2.689	816.9	16.7	781.32	17.9	681	57	-16.6
	11	191.9	422.8	0.5	0.133552	2.468	1.162148	4.180	0.063112	3.431	808.1	18.7	781.32	22.8	712	73	-11.9
	12	144.7	374.7	0.4	0.142045	2.974	1.318356	4.051	0.067314	2.821	856.2	23.8	781.32	23.4	848	59	-1.0
	13	166.7	343.0	0.5	0.135166	2.348	1.219335	2.638	0.065427	1.300	817.3	18.0	781.32	14.7	788	27	-3.6
	14	196.5	387.4	0.5	0.131838	2.373	1.137224	3.814	0.062561	3.026	798.3	17.8	781.32	20.6	693	65	-13.2
	15	209.4	458.2	0.5	0.137948	2.685	1.206108	3.162	0.063411	1.740	833.1	21.0	781.32	17.6	722	37	-13.3
	16	116.5	341.0	0.3	0.159848	2.799	1.383092	4.001	0.062754	2.976	955.9	24.9	781.32	23.6	700	63	-26.8
	17	121.5	258.9	0.5	0.141130	2.729	1.295142	2.896	0.066558	1.275	851.0	21.8	781.32	16.6	824	27	-3.2
	18	310.1	1186.3	0.3	0.120088	3.459	1.086051	3.598	0.065592	1.290	731.1	23.9	781.32	19.0	793	27	8.5
	19	117.3	252.4	0.5	0.142106	2.207	1.213447	3.923	0.061931	3.348	856.6	17.7	781.32	21.8	672	72	-21.6
	20	457.3	404.8	1.1	0.098571	2.900	0.846611	3.994	0.062292	2.889	606.0	16.8	781.32	18.6	684	62	12.9
	21	174.1	321.6	0.5	0.140117	2.640	1.269865	2.883	0.065730	1.287	845.3	20.9	781.32	16.4	798	27	-5.6
	22	92.3	215.6	0.4	0.146406	2.576	1.340076	3.030	0.066385	1.690	880.8	21.2	781.32	17.6	819	35	-7.1
	23	184.5	469.5	0.4	0.136522	3.021	1.160564	4.930	0.061654	3.936	825.0	23.4	781.32	26.9	662	84	-19.7
	24	213.5	511.6	0.4	0.131693	2.445	1.184465	3.329	0.065231	2.338	797.5	18.3	781.32	18.3	782	49	-2.0

Spot	Cone. (ppm)				Ratios						Ages					
	[U]	[Th]	U/Th	$^{206}\text{Pb} / ^{238}\text{U}$	$2\sigma$	$^{207}\text{Pb} / ^{235}\text{U}$	$2\sigma$	$^{207}\text{Pb} / ^{230}\text{ePb}$	$2\sigma$	$^{206}\text{Pb} / ^{238}\text{U}$	$2\sigma$	$^{206}\text{Pb} / ^{238}\text{U}$	$2\sigma$	$^{206}\text{Pb} / ^{238}\text{U}$	$2\sigma$	%Disc
25	124.0	364.9	0.3	0.142620	2.540	1.289803	3.014	0.065591	1.699	859.5	20.4	781.32	17.2	793	36	-7.7
26	573.7	2043.7	0.3	0.092512	4.723	0.789939	5.257	0.061929	2.364	570.4	25.8	781.32	23.6	672	51	17.8
27	336.6	161.1	2.1	0.135464	1.951	1.213451	2.255	0.064968	1.236	819.0	15.0	781.32	12.6	773	26	-5.6
28	174.9	324.1	0.5	0.138014	2.462	1.245291	2.902	0.065441	1.560	833.4	19.2	781.32	16.3	789	33	-5.4
29	199.4	428.1	0.5	0.137062	1.896	1.210868	4.273	0.064073	3.836	828.0	14.7	781.32	23.8	744	81	-10.1
30	64.0	152.4	0.4	0.141190	1.975	1.288397	2.423	0.066183	1.422	851.4	15.8	781.32	13.9	812	30	-4.6
31	529.4	1470.2	0.4	0.276919	1.887	3.733770	4.153	0.097790	4.443	1575.8	26.4	781.32	33.3	1582	83	0.4
32	137.4	251.0	0.5	0.138969	2.534	1.194278	5.605	0.062328	5.055	838.8	19.9	781.32	31.0	685	108	-18.3
33	205.5	580.8	0.4	0.127853	2.436	1.122027	5.850	0.063649	5.372	775.6	17.8	781.32	31.4	730	114	-5.9
34	254.1	438.3	0.6	0.136883	2.801	1.221146	6.035	0.064702	5.331	827.0	21.7	781.32	33.7	765	112	-7.5
35	130.6	209.7	0.6	0.142690	2.842	1.238597	6.327	0.062956	5.639	859.9	22.9	781.32	35.6	707	120	-17.8
36	156.7	281.1	0.6	0.132944	2.969	1.163072	6.332	0.063451	5.579	804.6	22.5	781.32	34.6	723	118	-10.1
37	161.7	554.1	0.3	0.129180	3.024	1.152426	6.054	0.064702	5.230	783.2	22.3	781.32	32.9	765	110	-2.4
38	223.0	436.3	0.5	0.135237	2.719	1.183805	6.873	0.063487	6.300	817.7	20.9	781.32	37.8	725	134	-11.4
39	437.8	972.6	0.5	0.120545	2.064	1.065678	5.188	0.064117	4.915	733.7	14.3	781.32	27.2	746	104	-1.6
40	416.2	148.7	2.8	0.126116	2.010	1.115021	5.330	0.064123	5.086	765.7	14.5	781.32	28.5	746	107	-2.6
41	139.5	263.4	0.5	0.136731	2.386	1.198113	5.201	0.063552	4.781	826.1	18.5	781.32	28.8	727	101	-12.0
42	458.1	233.0	2.0	0.119949	2.512	1.069647	4.281	0.064676	3.694	730.3	17.3	781.32	22.5	764	78	4.6
43	35.6	45.6	0.8	0.135391	3.747	1.174845	18.259	0.062934	18.225	818.5	28.8	781.32	100.5	706	388	-13.7
44	308.8	663.4	0.5	0.111858	4.756	0.983298	4.015	0.063755	5.257	683.5	30.8	781.32	20.2	734	111	7.3
45	279.4	565.0	0.5	0.128539	4.618	1.158841	3.013	0.065386	4.678	779.5	33.9	781.32	16.4	787	98	0.9
46	177.4	353.4	0.5	0.140974	4.945	1.286542	3.454	0.066189	4.648	850.2	39.4	781.32	19.7	812	97	-4.4
47	215.2	524.8	0.4	0.137912	4.563	1.234958	3.581	0.064946	5.112	832.8	35.7	781.32	20.1	773	108	-7.2
48	134.3	529.3	0.3	0.129015	4.990	1.101421	7.741	0.061917	8.316	782.2	36.8	781.32	41.2	671	178	-14.2
49	159.6	331.7	0.5	0.135524	4.798	1.186464	6.132	0.063494	6.737	819.3	36.9	781.32	33.8	725	143	-11.5
50	109.0	301.1	0.4	0.147093	4.524	1.328958	4.108	0.065527	5.216	884.6	37.4	781.32	23.8	791	109	-10.6
51	221.4	406.8	0.5	0.121225	3.741	1.087277	3.002	0.065050	3.835	737.6	26.1	781.32	15.9	776	81	5.2
52	253.7	508.8	0.5	0.140399	3.867	1.243727	5.840	0.064248	5.458	846.9	30.7	781.32	32.9	750	115	-11.5
53	91.5	154.9	0.6	0.139356	3.785	1.263152	5.821	0.065740	5.496	841.0	29.8	781.32	33.0	798	115	-5.1
54	175.8	399.7	0.4	0.141702	2.698	1.265509	8.475	0.064772	7.728	854.3	21.6	781.32	48.1	767	163	-10.2
55	194.4	452.6	0.4	0.142516	2.557	1.280496	8.294	0.065165	7.578	858.9	20.6	781.32	47.3	780	159	-9.2
56	269.9	663.4	0.4	0.120905	2.193	1.045737	8.211	0.062730	7.602	735.8	15.2	781.32	42.6	699	162	-5.0

Spot	Cone. (ppm)				Ratios						Ages					
	[U]	[Th]	U/Th	$^{206}\text{Pb} / ^{238}\text{U}$	$2\sigma$	$^{207}\text{Pb} / ^{235}\text{U}$	$2\sigma$	$^{207}\text{Pb} / ^{230}\text{Pb}$	$2\sigma$	$^{206}\text{Pb} / ^{238}\text{U}$	$2\sigma$	$^{206}\text{Pb} / ^{238}\text{U}$	$2\sigma$	$^{206}\text{Pb} / ^{238}\text{U}$	$2\sigma$	%Disc
57	85.4	165.0	0.5	0.137376	2.251	1.248098	8.751	0.065893	8.167	829.8	17.5	781.32	49.4	803	171	-3.2
58	153.4	222.4	0.7	0.136762	2.301	1.253382	6.591	0.066469	5.942	826.3	17.8	781.32	37.2	821	124	-0.6
59	303.9	554.1	0.5	0.136144	2.012	1.205911	7.692	0.064241	7.177	822.8	15.5	781.32	42.7	750	152	-8.9
60	179.9	201.3	0.9	0.329333	2.905	5.560603	8.089	0.122458	7.306	1835.1	46.4	781.32	69.7	1992	130	8.6
61	200.6	444.7	0.5	0.136737	2.005	1.226169	7.696	0.065037	7.183	826.2	15.5	781.32	43.1	776	151	-6.1
62	71.1	220.4	0.3	0.143735	2.073	1.249003	9.018	0.063023	8.568	865.7	16.8	781.32	50.9	709	182	-18.1
63	199.0	366.3	0.5	0.139613	2.507	1.261393	7.832	0.065528	7.172	842.5	19.8	781.32	44.4	791	150	-6.1

## APPENDIX B - Zircon Data Tables

**Table B.1: 5-30-02-3A**

Spot	Cone. (ppm)				Ratios						Ages					
	[U]	[Th]	U/Th	$^{206}\text{Pb} / ^{238}\text{U}$	$2\sigma$	$^{207}\text{Pb} / ^{235}\text{U}$	$2\sigma$	$^{207}\text{Pb} / ^{230}\text{Pb}$	$2\sigma$	$^{206}\text{Pb} / ^{238}\text{U}$	$2\sigma$	$^{206}\text{Pb} / ^{238}\text{U}$	$2\sigma$	$^{206}\text{Pb} / ^{238}\text{U}$	$2\sigma$	%Disc
1	37744.7	35827.8	1.1	0.39673	2.301	6.88206	2.971	0.1258	1.956	2154.0	42.1	2096.35	26.3	2040	35	-5.3
2	168041.5	122274.8	1.4	0.06536	2.148	0.50129	7.681	0.05562	7.394	408.2	8.5	412.58	26.0	437	165	7.1
3	104444.2	66593.7	1.6	0.17586	2.367	1.65549	6.711	0.06827	6.282	1044.3	22.8	991.65	42.5	877	130	-16.0
4	143223.0	83423.0	1.7	0.08351	2.367	0.65677	7.195	0.05703	6.792	517.0	11.8	512.64	29.0	493	150	-4.6
5	253354.8	17355.1	14.6	0.32126	3.265	4.85753	3.481	0.10966	1.198	1795.9	51.2	1794.9	29.3	1794	22	-0.1
6	137535.0	61861.0	2.2	0.07068	2.255	0.54476	2.096	0.0558	1.380	440.3	9.6	441.56	7.5	448	31	1.8
7	194411.0	188671.0	1.0	0.06806	2.511	0.73006	7.225	0.07779	5.816	424.5	10.3	556.59	31.0	1142	116	169.0
8	81694.0	62452.2	1.3	0.07068	2.256	0.54234	3.233	0.05565	2.285	440.3	9.6	439.97	11.5	438	51	-0.4
9	115819.4	140681.7	0.8	0.09078	2.356	0.69067	6.387	0.05517	5.924	560.2	12.6	533.21	26.5	419	132	-25.1
10	184587.1	979513.0	0.2	0.08854	8.619	0.67443	99.179	0.05524	98.803	546.9	45.2	523.40	429.5	422	2205	-22.8
11	235775.0	192616.0	1.2	0.05954	2.017	0.61876	3.087	0.07537	3.652	372.8	7.3	489.08	12.0	1078	73	189.2
12	60288.0	39115.0	1.5	0.16505	1.884	1.63260	1.520	0.07173	1.934	984.8	17.2	982.86	9.6	979	39	-0.6
13	78591.7	32343.7	2.4	0.18640	2.047	1.70534	6.404	0.06635	6.116	1101.8	20.7	1010.5	41.0	818	128	-25.8
14	128746.0	64424.0	2.0	0.07037	2.208	0.54222	2.223	0.05587	1.466	438.4	9.4	439.89	7.9	447	33	2.1
15	165456.0	108798.0	1.5	0.06845	2.044	0.55679	2.059	0.05898	1.457	426.9	8.4	449.44	7.5	567	32	32.8
16	33401.5	19130.1	1.7	0.56398	2.134	15.46342	3.035	0.19885	3.043	2883.1	49.6	2844.23	28.9	2817	50	-2.3
17	239394.5	155801.7	1.5	0.06214	2.638	0.48361	8.015	0.05644	7.866	388.6	10.0	400.55	26.5	470	174	20.9
18	81694.0	61532.0	1.3	0.07354	2.927	0.63553	4.435	0.06267	3.732	457.5	12.9	499.5	17.5	697	80	52.4
19	252837.8	67119.7	3.8	0.34388	2.317	6.963186	3.007	0.14685	2.876	1905.3	38.2	2106.75	26.7	2310	49	21.2
20	107029.0	107812.0	1.0	0.06761	2.284	0.54041	2.767	0.05796	3.214	421.8	9.3	438.70	9.9	528	70	25.3
21	438459.0	239948.0	1.8	0.06647	1.998	0.50969	2.557	0.05561	2.438	414.9	8.0	418.24	8.8	437	54	5.5
22	112200.0	81188.0	1.4	0.07144	2.205	0.54539	3.053	0.05536	2.673	444.9	9.5	441.9	10.9	427	60	-4.0
23	197513.4	126284.9	1.6	0.070214	2.314	0.52102	3.416	0.05381	2.758	437.4	9.8	425.83	11.9	363	62	-16.9
24	227502.3	113071.3	2.0	0.19301	2.141	2.02557	4.043	0.07611	3.347	1137.7	22.3	1124.13	27.5	1098	67	-3.5

Spot	Cone. (ppm)				Ratios						Ages					
	[U]	[Th]	U/Th	$^{206}\text{Pb} / ^{238}\text{U}$	$2\sigma$	$^{207}\text{Pb} / ^{235}\text{U}$	$2\sigma$	$^{207}\text{Pb} / ^{230}\text{Pb}$	$2\sigma$	$^{206}\text{Pb} / ^{238}\text{U}$	$2\sigma$	$^{206}\text{Pb} / ^{238}\text{U}$	$2\sigma$	$^{206}\text{Pb} / ^{238}\text{U}$	$2\sigma$	%Disc
25	73473.0	41810.0	1.8	0.07366	2.154	0.57135	3.081	0.05625	2.822	458.2	9.5	458.89	11.4	462	63	0.9
26	193015.0	274132.2	0.7	0.239581	3.390	3.439985	4.730	0.104137	3.099	1384.5	42.2	1513.58	37.2	1699	57	22.7
27	207854.4	114386.1	1.8	0.28551	2.098	4.61425	3.767	0.11721	2.917	1619.1	30.0	1751.85	31.4	1914	52	18.2
28	115302.3	66659.5	1.7	0.17031	2.061	1.59682	5.554	0.06799	5.032	1013.8	19.3	968.9	34.7	869	104	-14.3
29	46120.9	18538.4	2.5	0.52106	2.004	12.547570	3.676	0.17464	2.866	2703.7	44.2	2646.30	34.6	2603	48	-3.7
30	119955.8	74088.0	1.6	0.165760	2.131	1.61005	3.815	0.07044	2.992	988.7	19.5	974.13	23.9	7941	61	-4.8
31	220263.6	611373.9	0.4	0.06082	2.269	0.44611	14.802	0.05319	14.546	380.6	8.4	374.56	46.4	337	330	-11.4
32	390373.3	115963.8	3.4	0.16272	2.181	1.57541	3.238	0.07021	1.833	971.9	19.7	960.56	20.1	935	38	-3.8
33	199064.5	205106.1	1.0	0.069846	2.589	0.519738	3.386	0.053969	1.844	435.2	10.9	424.98	11.8	370	42	-15.0
34	465345.6	456229.6	1.0	0.132471	2.902	1.224032	4.375	0.067015	3.042	801.9	21.9	811.62	24.5	838	63	4.5
35	39709.5	18965.7	2.1	0.16996	1.721	1.69725	3.022	0.07242	2.170	1011.9	16.1	1007.5	19.3	998	44	-1.4
36	146325.0	194588.0	0.8	0.06777	2.317	0.84982	4.066	0.09093	3.435	422.8	9.5	624.55	19.0	1445	65	241.9
37	227502.0	129506.0	1.8	0.07214	2.011	0.55874	3.043	0.05616	1.582	449.1	8.7	450.71	11.1	459	35	2.2
38	215610.1	216281.7	1.0	0.06977	1.757	0.52519	3.103	0.05458	2.098	434.8	7.4	428.62	10.9	395	47	-9.1
39	170110.0	147519.0	1.2	0.06515	1.741	0.53075	2.848	0.05908	2.004	406.9	6.9	432.31	10.0	570	44	40.1
40	159768.7	102553.0	1.6	0.07098	2.695	0.51800	10.412	0.05292	9.989	442.1	11.5	423.82	36.1	326	227	-26.4
41	201132.7	130820.9	1.5	0.121764	2.321	1.112848	3.433	0.066285	2.248	740.7	16.2	759.54	18.4	815	47	10.1
42	283343.8	65666.8	4.3	0.166450	2.127	1.623950	2.736	0.070760	1.271	992.5	19.6	979.52	17.2	950	26	-4.2
43	221298.0	159089.0	1.4	0.071497	2.441	0.572748	2.639	0.058100	1.532	445.2	10.5	459.79	9.8	534	34	19.8
44	125643.3	56253.0	2.2	0.372763	4.496	8.660625	5.259	0.168506	2.613	2042.4	78.7	2302.95	47.9	2543	44	24.5
45	75851.3	55746.8	1.4	0.073600	1.660	0.568111	7.301	0.055983	7.067	457.8	7.3	456.79	26.9	452	157	-1.3
46	83090.0	80333.2	1.0	0.211299	1.701	2.369059	2.150	0.081316	1.329	1235.7	19.1	1233.32	15.4	1229	26	-0.5
47	317986.2	184069.6	1.7	0.069277	1.923	0.517021	2.329	0.054127	1.328	431.8	8.0	423.16	8.1	376	30	-12.8
48	87123.0	26131.0	3.3	0.131802	1.592	1.212625	1.891	0.66727	1.570	798.1	11.9	806.40	10.5	829	33	3.9
49	232414.0	149425.0	1.6	0.057183	1.757	0.468949	2.085	0.059478	1.926	358.5	6.1	390.46	6.8	585	42	63.1
50	270003.9	48121.0	5.6	0.171732	1.693	1.776384	2.128	0.075021	1.304	1021.6	16.0	1036.86	13.8	1069	26	4.6
51	146325.3	207735.7	0.7	0.123527	2.248	1.035370	4.944	0.060790	4.520	750.8	15.9	721.61	25.5	632	97	-15.9
52	45759.0	60611.0	0.8	0.094316	2.161	1.189978	2.446	0.091507	2.262	581.0	12.0	795.95	13.5	1457	43	150.8
53	95654.4	55549.6	1.7	0.271727	3.095	3.935026	3.236	0.105030	1.389	1549.6	42.6	1620.91	26.2	171	26	10.7
54	156149.0	80859.0	1.9	0.075159	2.699	0.586338	2.715	0.056580	1.469	467.2	12.2	468.53	10.2	475	32	1.7
55	122282.5	78689.7	1.6	0.192389	1.983	1.987479	2.180	0.074924	1.135	1134.3	20.6	1111.27	14.7	1066	23	-6.0
56	245599.1	78887.0	3.1	0.276670	1.929	3.836344	1.918	0.100567	1.249	1574.6	26.9	1600.41	15.5	1635	23	3.8

Spot	Cone. (ppm)				Ratios						Ages					
	[U]	[Th]	U/Th	$^{206}\text{Pb} / ^{238}\text{U}$	$2\sigma$	$^{207}\text{Pb} / ^{235}\text{U}$	$2\sigma$	$^{207}\text{Pb} / ^{230}\text{Pb}$	$2\sigma$	$^{206}\text{Pb} / ^{238}\text{U}$	$2\sigma$	$^{206}\text{Pb} / ^{238}\text{U}$	$2\sigma$	$^{206}\text{Pb} / ^{238}\text{U}$	$2\sigma$	%Disc
57	110132.0	146598.0	0.8	0.076675	3.066	0.626558	2.645	0.059266	1.778	476.2	14.1	493.95	10.3	577	39	21.1
58	176727.9	188671.3	0.9	0.068533	2.200	0.499021	8.358	0.052810	8.162	427.3	9.1	411.04	28.3	321	185	-25.0
59	89708.3	65147.5	1.4	0.073284	2.084	0.539555	4.961	0.053398	4.676	455.9	9.2	438.13	17.7	346	106	-24.2
60	284377.9	138643.8	2.1	0.069069	1.835	0.522868	3.278	0.054905	2.871	427.3	9.1	427.07	11.4	408	64	-5.2
61	170109.7	59428.2	2.9	0.232043	2.290	2.833139	2.715	0.088552	1.522	1345.2	27.8	1364.35	20.4	1394	29	3.7
62	219747.0	59165.0	3.7	0.144333	2.129	1.391618	2.011	0.069928	1.258	869.1	17.3	885.38	11.9	926	26	6.6
63	219746.5	59165.2	3.7	0.144022	2.135	1.359392	3.113	0.068457	2.307	867.4	17.3	871.61	18.2	882	48	1.7
64	296270.0	136014.3	2.2	0.069329	1.808	0.517752	3.346	0.054163	2.942	432.1	7.6	423.65	11.6	378	66	-12.6
65	109356.0	80005.0	1.4	0.075776	2.117	0.593337	2.135	0.056789	1.627	470.9	9.6	473.00	8.1	483	36	2.7
66	100049.0	43348.0	2.3	0.139055	2.357	1.637072	3.572	0.085385	2.181	839.3	18.6	984.59	22.5	1324	42	57.8
67	16182.3	32080.7	5.0	0.153855	1.840	1.464343	2.504	0.069029	1.825	922.5	15.8	915.80	15.1	900	38	-2.5
68	220264.0	136080.0	1.6	0.074493	4.074	0.569861	4.116	0.055482	1.649	463.2	18.2	457.92	15.2	432	37	-6.8
69	270418.0	232059.0	1.2	0.108520	6.026	1.491164	9.410	0.099658	5.127	664.1	38.0	926.79	57.3	528	44	8.8
70	71870.0	51211.0	1.4	0.078150	1.773	0.624359	2.210	0.057943	1.990	485.1	8.3	492.58	8.6	528	44	8.8
71	119439.0	47332.0	2.5	0.076707	2.520	0.588836	2.449	0.055675	1.489	476.4	11.6	470.12	9.2	439	33	-7.8
72	229725.6	22285.6	10.3	0.152736	2.053	1.416653	2.537	0.067270	1.667	916.3	17.5	895.96	15.1	846	35	-7.7
73	126522.3	62912.3	2.0	0.168680	2.115	1.621813	2.568	0.069733	1.644	1004.8	19.7	978.69	16.1	920	34	-8.4
74	52067.0	44702.6	1.2	0.086233	5.138	0.705229	15.405	0.059313	14.532	533.2	26.3	541.91	64.8	579	316	8.5
75	56358.5	22088.3	2.6	0.416986	1.902	8.626633	2.279	0.150044	1.355	2246.8	36.1	2299.37	20.7	2346	23	4.4
76	236292.2	203462.6	1.2	0.069366	1.666	0.510563	6.806	0.053383	6.607	432.3	7.0	418.83	23.4	345	149	-20.2
77	235775.1	118987.8	2.0	0.073963	1.825	0.541323	4.437	0.053081	4.057	460.0	8.1	439.30	15.8	332	92	-27.8
78	201132.7	141273.4	1.4	0.074267	2.242	0.545235	5.894	0.053246	5.461	461.8	10.0	441.87	21.1	339	124	-26.5
79	150978.8	102750.3	1.5	0.163720	1.917	1.538862	4.065	0.068171	3.600	977.4	17.4	946.05	25.0	874	75	-10.6
80	389339.2	20273.9	19.2	0.093542	1.900	0.772532	3.235	0.059897	2.586	576.5	10.5	581.21	14.3	600	56	4.1
81	40692.0	18177.0	2.2	0.179233	1.897	1.925589	2.208	0.077919	2.282	1062.8	18.6	1090.01	14.8	1145	45	7.7
82	103358.0	58113.0	1.8	0.075617	1.776	0.631252	2.279	0.060545	1.958	469.9	8.0	496.88	9.0	623	42	32.6
83	140638.0	64359.0	2.2	0.079074	2.478	0.614889	2.420	0.056398	1.753	490.6	11.7	486.64	9.4	468	39	-4.6
84	103565.0	89077.0	1.2	0.075118	1.740	0.577051	2.243	0.055715	1.861	466.9	7.8	462.56	8.3	441	41	-5.5
85	214576.0	173551.3	1.2	0.071174	2.223	0.555813	5.351	0.056638	4.963	443.2	9.5	448.80	19.4	477	110	7.7
86	323674.0	150543.0	2.2	0.068272	1.961	0.576019	1.996	0.061192	1.821	425.7	8.1	461.90	7.4	646	39	51.7
87	219229.0	199190.0	1.1	0.077321	1.856	0.745361	2.562	0.069915	2.012	480.1	8.6	565.53	11.1	926	41	92.8
88	98240.0	84278.0	1.2	0.077661	2.213	0.602174	2.571	0.056236	1.765	482.1	10.3	478.61	9.8	462	39	-4.2

Spot	Cone. (ppm)				Ratios						Ages						
	[U]	[Th]	U/Th	$^{206}\text{Pb} / ^{238}\text{U}$	$2\sigma$	$^{207}\text{Pb} / ^{235}\text{U}$	$2\sigma$	$^{207}\text{Pb} / ^{230}\text{Pb}$	$2\sigma$	$^{206}\text{Pb} / ^{238}\text{U}$	$2\sigma$	$^{206}\text{Pb} / ^{238}\text{U}$	$2\sigma$	$^{206}\text{Pb} / ^{238}\text{U}$	$2\sigma$	%Disc	
89	191309.0	145283.0	1.3	0.081705	3.123	0.644059	3.855	0.057171	1.509	506.3	15.2	504.82	15.3	498	33	-1.6	
90	166490.0	104788.0	1.6	0.076083	2.385	0.679097	3.621	0.064735	2.603	472.7	10.9	526.23	14.9	766	55	62.0	
91	363487.0	68369.0	5.3	0.084499	3.036	0.854632	3.684	0.073355	1.677	522.9	15.2	627.19	17.2	1024	34	95.8	
92	284894.9	773749.6	0.4	0.086097	2.053	0.665474	4.398	0.056058	3.949	532.4	10.5	517.96	17.8	455	88	-14.6	
93	90587.0	97491.0	0.9	0.076480	2.404	0.662491	3.833	0.062825	2.467	475.1	11.0	516.14	15.5	702	53	47.8	
94	96999.0	153172.0	0.6	0.075707	2.131	0.720420	2.412	0.069015	2.526	470.4	9.7	550.91	10.3	899	52	91.1	
95	584.0	2932.0	0.2	9.653360	4.799	1106.614073	5.117	0.831412	1.399	15251.4	280.5	7117.80	52.0	4977	20	-67.4	
<b>51</b>	96	97309.0	63898.0	1.5	0.118027	2.549	1.233212	3.350	0.075780	3.321	719.2	17.3	815.80	18.8	1089	67	51.5
	97	59460.8	11701.6	5.1	0.133976	3.283	1.175173	5.188	0.063617	3.224	810.5	25.0	789.06	28.5	729	68	-10.1

## APPENDIX C - Zircon Data Tables

**Table C.1: 6-29-02-3**

Spot	Cone. (ppm)				Ratios						Ages					
	[U]	[Th]	U/Th	$^{206}\text{Pb} / ^{238}\text{U}$	$2\sigma$	$^{207}\text{Pb} / ^{235}\text{U}$	$2\sigma$	$^{207}\text{Pb} / ^{230}\text{Pb}$	$2\sigma$	$^{206}\text{Pb} / ^{238}\text{U}$	$2\sigma$	$^{206}\text{Pb} / ^{238}\text{U}$	$2\sigma$	$^{206}\text{Pb} / ^{238}\text{U}$	$2\sigma$	%Disc
1	1537	2339	0.70	0.102637	4016.814	1.396761	40116.718	0.098700	40115.330	629.8	40100.9	887.56	40842.2	1600	402152	154.0
2	383	264	1.50	0.301657	407.424	3.784360	4032.987	0.090987	4030.816	1699.5	40110.9	1589.43	40271.2	1446	40587	-14.9
3	951	906	1.00	0.087501	4014.641	1.417265	4077.222	0.117473	4074.011	540.7	4075.9	896.21	40495.7	1918	401327	254.7
4	939	892	1.10	0.057984	13.533	0.850338	4075.689	0.106360	4073.521	363.4	4047.8	624.83	40368.6	1738	401348	378.3
5	2722	1262	2.20	0.069192	407.425	0.479098	4032.937	0.050219	4030.746	431.3	4031.0	40397.45	40108.7	205	40713	-52.4
6	555	854	0.60	0.149154	4012.415	1.684067	4099.069	0.081889	4097.858	896.2	40103.9	1002.52	40738.8	1243	401917	38.7
7	242	169	1.40	0.107445	4022.206	1.703239	40124.646	0.114971	40122.651	657.9	40138.9	1009.75	401075.5	1879	402210	185.7
8	679	2175	0.30	0.088954	4012.092	1.294965	4080.734	0.105583	4079.822	549.3	4063.7	843.50	40499.2	1724	401466	213.9
9	1484	1217	1.20	0.068529	4010.474	0.961937	4071.221	0.101800	4070.446	427.3	4043.3	684.30	40370.1	1657	401305	287.9
10	2122	1348	1.60	0.067498	406.598	0.524409	4082.555	0.056348	4082.288	421.1	4026.9	428.09	40296.5	466	401823	10.7
11	1778	2998	0.60	0.0942	15.783	400.870	170.650	0.060669	169.919	40580.6	87.6	635.69	401	837	403.5	44.1
12	2806.5	1102	2.5	0.14677	402.235	1.225744	409.265	0.060571	408.986	882.8	4018.4	812.4	4051.9	624	40194-	29.3
13	1825.7	2593.5	0.7	400.10643	10.035	401.2219	4089.05	0.0832	4088.48	652	4062.2	810.67	40544	1276	40172	95.6
14	1842.3	3301.7	0.6	0.112387	4012.388	1.94472	4070.149	0.125498	4069.046	686.6	4080.7	1096.63	509.2	2036	1221	196.5
15	1895.3	3410	0.6	0.094263	14.753	0.664806	213.86	0.051151	213.351	580.7	81.9	517.55	1290.3	248	4912	-57.4
16	642.8	1235.3	0.5	0.099421	12.319	1.292694	92.305	0.094301	91.485	611	71.8	842.49	585.8	1514	1726	147.8
17	2054.3	1976.9	0.152155	13.705	1.798728	119.413	0.085739	118.553	913	116.7	1045	1029.7	1332	2293	45.9	24
18	1030.5	1385.3	0.7	0.077071	13.042	0.973735	100.314	0.091632	99.391	478.6	60.2	690.39	550.9	1460	1889	205
19	629.5	156	4	0.279024	3.848	4.022274	16.822	0.104551	14.429	1586.4	54.1	1638.71	137.6	1706	266	7.6
20	255.1	450	0.6	0.160523	14.558	3.569393	61.838	0.16127	59.599	959.7	129.8	1542.75	535.1	2469	1006	157.3
21	1297.2	3441.3	0.4	0.078606	12.758	0.83611	117.553	0.077145	116.602	487.8	59.9	617	606.7	1125	2324	130.6
22	6179.5	13956.8	0.4	0.198684	2.923	2.195013	11.553	0.080126	9.512	1168.2	31.2	1179.46	80.8	1200	188	2.7
23	113.3	266.6	0.4	0.156648	23.489	2.984406	110.684	0.138176	108.073	938.1	205.1	1403.65	1203.3	2204	1876	135
24	1275.7	1029.1	1.2	0.464549	2.985	10.260681	3.322	0.160193	1.846	2459.6	61	2458.56	30.7	2458	31	-0.1

Cone.	Ratios										Ages					
	[U]	[Th]	U/Th	$^{206}\text{Pb} / ^{238}\text{U}$	$2\sigma$	$^{207}\text{Pb} / ^{235}\text{U}$	$2\sigma$	$^{207}\text{Pb} / ^{230}\text{Pb}$	$2\sigma$	$^{206}\text{Pb} / ^{238}\text{U}$	$2\sigma$	$^{206}\text{Pb} / ^{238}\text{U}$	$2\sigma$	$^{206}\text{Pb} / ^{238}\text{U}$	$2\sigma$	%Disc
25	472.2	776.2	0.6	0.072825	10.762	1.015027	71.155	0.101088	70.346	453.2	47.1	711.41	380.9	1644	1305	262.8
26	964.2	824.9	1.2	0.076737	17.716	0.643426	206.607	0.060813	205.849	476.6	81.4	504.43	1141.1	633	4433	32.7
27	111	95.2	1.2	0.261598	21.954	10.302201	49.265	0.285624	44.117	1498	293.7	2462.3	491	3394	687	126.6
28	613	1131.1	0.5	0.082468	14.312	0.93415	118.263	0.082154	117.401	510.8	70.3	669.82	659.3	1249	2298	144.5
29	4224.6	1014.5	4.2	0.163533	9.817	1.494982	10.478	0.066302	3.606	976.4	89	928.35	63.8	816	75	-16.4
30	493.7	6.6	74.3	0.080475	7.596	0.698625	44.397	0.062962	43.716	499	36.5	537.97	187.5	707	930	41.7
31	366.1	610.4	0.6	0.106764	17.276	1.364527	123.647	0.092695	122.425	653.9	107.4	873.82	908.1	1482	2320	126.6
31	3311.7	937.2	3.5	0.068988	9.849	0.447518	15.502	0.047047	11.901	430.1	41	375.54	48.7	52	284	-88
32	5997.3	2960.1	2	0.130273	10.169	1.102319	11.192	0.061369	4.493	789.4	75.6	754.47	59.7	652	96	-17.4
33	2654	2524.7	1.1	0.097427	16.571	1.113515	118.152	0.082892	116.977	599.3	94.8	759.86	740.3	1267	2284	111.4
34	2029.5	1318.6	1.5	0.104819	18.789	1.716068	108.349	0.118738	106.718	642.6	114.9	1014.56	850.6	1937	1910	201.5
35	5997.3	1531.1	3.9	0.238531	2.919	4.874784	3.217	0.148221	1.997	1379.1	36.2	1797.91	27.1	2326	34	68.6
36	1958.2	1320.7	1.5	0.331034	2.538	4.948334	4.198	0.108414	3.458	1843.4	40.7	1810.54	35.5	1773	63	-3.8
37	1852.2	2358.1	0.8	0.088529	9.305	1.045006	78.46	0.085611	77.906	546.8	48.8	726.41	431.3	1329	1508	143.1
38	2798.2	1479	1.9	0.153394	2.47	1.371767	6.925	0.064859	6.462	920	21.2	876.92	40.7	770	136	-16.3
39	1086.8	42.1	25.8	0.078823	11.288	0.633216	128.688	0.058264	128.184	489.1	53.2	498.1	556.3	540	2804	10.3
40	13170.8	4051.6	3.3	0.288848	2.493	4.328451	3.048	0.108683	1.064	1635.8	36	1698.8	25.1	1777	19	8.7
41	2152.1	1164.5	1.8	0.252908	2.494	3.424935	4.017	0.098217	2.824	1453.5	32.4	1510.13	31.6	1591	53	9.4
42	2895.9	1273.4	2.3	0.666512	2.149	25.677229	2.663	0.279408	1.264	3292.4	55.4	3334.33	26	3360	20	2
43	7885.9	8605.3	0.9	0.150854	2.851	2.076703	6.356	0.099843	5.313	905.7	24.1	1141.15	43.6	1621	99	79
44	1809.1	727	2.5	0.344618	2.205	5.513772	3.864	0.116041	2.453	1908.8	36.4	1902.75	33.2	1896	44	-0.7
45	85.8	17.8	4.8	0.314823	15.911	6.056429	70.55	0.139524	68.724	1764.4	245.7	1984	712.6	2221	1191	25.9
46	2773.3	2674.7	1	0.081756	2.729	0.529842	19.838	0.047003	19.638	506.6	13.3	431.7	69.9	49	469	-90.3
47	2725.3	1060.3	2.6	0.039107	4.144	0.166189	54.158	0.030821	53.998	247.3	10.1	7156.11	78.5	-1077	1628	-535.4
48	4700.1	1165.7	4	0.062306	3.178	0.417103	11.996	0.048553	11.56	389.6	12	353.98	35.9	126	272	-67.6
49	62.5	18.8	3.3	0.30504	12.437	17.925514	18.716	0.4262	13.98	1716.3	187.4	2985.74	181.9	4004	209	133.3
50	45.6	20.5	2.2	0.314256	13.822	16.270174	23.774	0.375497	19.339	1761.6	213.1	2892.81	231.3	3814	293	116.5
51	3210.7	2578.9	1.2	0.298531	1.694	4.245161	2.602	0.103135	2.041	1684	25.1	1682.8	21.4	1681	38	-0.2
52	1221	454.7	2.7	0.210834	2.109	2.48226	10.957	0.08539	10.764	1233.3	23.7	1266.87	79.5	1324	208	7.4
53	3528.8	3543.4	1	0.126313	7.393	1.50591	62.146	0.086467	61.709	766.8	53.5	932.78	398.5	1349	1191	75.9
54	5168.9	3962.1	1.3	0.16480	2.125	1.562329	3.973	0.068744	3.403	983.6	19.4	955.39	24.6	891	70	-9.4
55	4174.9	1104	3.8	0.322926	2.474	4.785215	3.459	0.107472	2.579	1804	38.9	1782.31	29.1	1757	47	-2.6
56	2745.2	3695.4	0.7	0.065257	2.515	0.402255	21.281	0.044707	21.138	407.5	9.9	343.28	62.1	-72	517	-117.6

## Cone. (ppm)

## Ratios

## Ages

Spot	[U]	[Th]	U/Th	$^{206}\text{Pb} / ^{238}\text{U}$	$2\sigma$	$^{207}\text{Pb} / ^{235}\text{U}$	$2\sigma$	$^{207}\text{Pb} / ^{230}\text{Pb}$	$2\sigma$	$^{206}\text{Pb} / ^{238}\text{U}$	$2\sigma$	$^{206}\text{Pb} / ^{238}\text{U}$	$2\sigma$	$^{206}\text{Pb} / ^{238}\text{U}$	$2\sigma$	%Disc
57	2032.8	3564.2	0.6	0.117784	11.795	1.305093	107.975	0.080362	107.322	717.8	80.1	847.97	722	1206	2114	68
58	1961.5	2710.1	0.7	0.109459	9.468	1.152608	91.779	0.076371	91.282	669.6	60.2	778.47	546.2	1105	1825	65
59	2387.3	1262.4	1.9	0.070634	2.002	0.371376	19.252	0.038133	19.11	440	8.5	320.67	53	-476	506	-208.2
60	1393.3	4.2	330.3	0.333137	1.954	4.988679	3.596	0.108608	2.77	1853.6	31.5	1817.4	30.4	1776	51	-4.2

## APPENDIX D - Zircon Data Tables

**Table D.1: 6-27-02**

Spot	Cone. (ppm)				Ratios						Ages					
	[U]	[Th]	U/Th	$^{206}\text{Pb} / ^{238}\text{U}$	$2\sigma$	$^{207}\text{Pb} / ^{235}\text{U}$	$2\sigma$	$^{207}\text{Pb} / ^{230}\text{Pb}$	$2\sigma$	$^{206}\text{Pb} / ^{238}\text{U}$	$2\sigma$	$^{206}\text{Pb} / ^{238}\text{U}$	$2\sigma$	$^{206}\text{Pb} / ^{238}\text{U}$	$2\sigma$	% Disc
1	641	324	1.98	0.15979	2.526	2.709861	5.09	0.122997	4.191	955.6	22.4	1331.16	37.8	2000	74	109.3
2	1173	538	2.18	0.083511	3.145	2.057118	8.926	0.178656	8.285	517	15.6	1134.66	61.1	2640	138	410.7
3	143	74	1.94	0.334794	4.483	6.356555	4.189	0.137703	5.313	1861.6	72.5	2026.29	36.8	2199	92	18.1
4	1255	325	3.86	0.189994	3.204	6.681545	5.794	0.255056	6.572	1121.3	33.0	2070.18	51.2	3216	104	186.8
5	617	79	7.78	0.174209	2.810	2.757860	7.926	0.114815	8.221	1035.3	26.9	1344.21	59.1	1877	148	81.3
6	268	182	1.47	0.228344	2.620	5.450229	6.221	0.173110	7.497	1325.8	31.4	1892.79	53.4	2588	125	95.2
7	936	28	33.11	0.079213	4.861	0.619830	7.649	0.056751	8.292	491.4	23.0	489.74	29.7	482	183	-1.9
8	636	175	3.64	0.095481	3.836	0.985253	9.826	0.074839	12.944	587.9	21.6	696.30	49.6	1064	260	81.0
9	601	574	1.05	0.280745	4.239	4.119351	9.680	0.106418	12.767	1595.1	59.9	1658.15	79.2	1739	234	9.0
10	897	44	20.40	0.112267	3.684	1.870732	9.844	0.120853	12.979	685.9	24.0	1070.79	65.2	1969	231	187.0
11	121	153	0.80	0.069760	3.941	1.207866	16.046	0.125577	16.044	434.7	16.6	804.21	89.4	2037	284	368.6
12	694	153	4.52	0.146749	2.517	2.109129	7.042	0.104238	8.420	882.7	20.8	1151.79	48.5	1701	155	92.7
13	689	392	1.76	0.157709	2.554	1.890821	5.579	0.086955	7.035	944.0	22.4	1077.87	37.1	1359	136	44.0
14	1470	659	2.23	0.072457	2.442	1.110138	7.721	0.111121	8.333	450.9	10.6	758.24	41.3	1818	151	303.1
15	1071	448	2.39	0.148239	3.427	2.728219	5.605	0.133480	7.881	891.1	28.5	1336.17	41.7	2144	138	140.6
16	282	121	2.33	0.220283	3.917	8.987374	10.574	0.295904	9.312	1283.4	45.6	2336.72	96.9	3449	144	168.7
17	359	97	3.71	0.123823	4.541	1.304711	7.093	0.076421	6.654	752.5	32.3	847.80	40.8	1106	133	47.0
18	639	73	8.80	0.146136	2.861	1.372575	7.983	0.068121	9.450	879.3	23.5	877.27	46.9	872	196	-0.8
19	840	387	2.17	0.073951	3.279	0.936091	6.773	0.091807	6.364	459.9	14.6	670.83	33.3	1463	121	218.2
20	482	73	6.64	0.154219	6.332	3.223903	5.499	0.151616	6.318	924.6	54.5	1462.92	42.6	2364	108	155.7
21	74	80	0.93	0.087882	5.842	3.595446	10.598	0.296725	5.673	543.0	30.4	1548.53	84.4	3453	88	536.0
22	821	349	2.35	0.174078	6.615	3.303777	5.636	0.137647	5.557	1034.5	63.2	1481.94	44.0	2198	97	112.4
23	721	3	224.74	0.07368	3.379	0.734967	5.498	0.072346	4.904	458.3	14.9	559.46	23.7	996	100	117.3
24	776	86	9.06	0.181138	3.804	4.639792	8.397	0.185775	5.91	1073.2	37.6	1756.46	70.3	2705	98	152.1

Spot	Cone.	Ratios										Ages					
		[U]	[Th]	U/Th	$^{206}\text{Pb} / ^{238}\text{U}$	$2\sigma$	$^{207}\text{Pb} / ^{235}\text{U}$	$2\sigma$	$^{207}\text{Pb} / ^{230}\text{Pb}$	$2\sigma$	$^{206}\text{Pb} / ^{238}\text{U}$	$2\sigma$	$^{206}\text{Pb} / ^{238}\text{U}$	$2\sigma$	$^{206}\text{Pb} / ^{238}\text{U}$	$2\sigma$	
25	383	166	2.3	0.133913	4.151	5.050632	5.963	0.273541	5.414	810.1	31.6	1827.85	50.6	3326	85	310.6	
26	758	159	4.78	0.071339	4.108	0.98408	6.883	0.100046	5.335	444.2	17.6	695.69	34.7	1625	99	265.8	
27	1184	404	2.93	0.068497	3.946	0.985496	10.461	0.104347	9.085	427.1	16.3	696.42	52.8	1703	167	298.7	
28	239	306	0.78	0.073911	3.854	2.1117	3.306	0.207215	2.818	459.7	17.1	1152.63	22.8	2884	46	527.4	
29	946	553	1.71	0.132136	3.109	1.874556	3.936	0.102891	3.721	800	23.4	1072.14	26.1	1677	69	109.6	
30	243	153	1.59	0.081727	2.027	1.116805	5.469	0.099108	6.027	506.4	9.9	761.44	29.3	1607	112	217.4	
31	476	160	2.97	0.435173	1.962	10.414995	3.436	0.173578	3.444	2329	38.4	2472.38	31.8	2592	57	11.3	
32	960	301	3.19	0.078756	3.593	1.894498	12.875	0.174466	9.681	488.7	16.9	1079.16	85.8	2601	161	432.2	
33	1173	379	3.1	0.071663	2.082	1.0257	5.775	0.103806	6.367	446.2	9	716.77	29.7	1693	117	279.5	
34	1030	391	2.64	0.073068	3.001	1.058832	2.242	0.105099	2.711	454.6	13.2	733.25	11.7	1716	50	277.5	
35	217	78	2.78	0.175124	3.185	2.749563	2.604	0.113872	2.62	1040.3	30.6	1341.97	19.4	1862	47	79	
36	309	182	1.7	0.1161	4.898	1.317305	2.373	0.082291	4.939	708.1	32.8	853.33	13.7	1252	97	76.9	
56	17	665	14	46.86	0.071126	3.427	0.734288	4.23	0.074875	3.716	442.9	14.7	559.07	18.2	1065	75	140.5
	18	76	30	2.56	0.262587	3.6	9.58685	8.527	0.26479	7.177	1503.1	48.3	2395.91	78.673275	113	117.9	45
	39	409	199	2.06	0.223869	3.187	2.46191	3.072	0.079759	3.565	1302.3	37.6	1260.92	22.2	1191	70	-8.5
	40	1022	329	3.1	0.145933	2.845	2.019514	4.012	0.100367	5.434	878.1	23.4	1122.1	27.3	1631	101	85.7
	41	620	165	3.76	0.130342	2.97	1.627111	6.287	0.090538	4.601	789.8	22.1	980.74	39.6	1437	88	81.9
	42	383	623	0.62	0.249725	2.991	3.012749	4.146	0.087498	3.262	1437.1	38.5	1410.85	31.6	1371	63	-4.6
	43	224	223	1	0.144883	8.657	2.9071	30.712	0.145526	12.567	872.2	70.6	1383.76	236.2	2294	216	163
	44	792	561	1.41	0.069918	2.19	0.60456	13.522	0.062712	13.997	435.7	9.2	480.12	51.8	698	298	60.3
	45	780	51	15.43	0.311589	7.121	21.770909	21.163	0.506749	19.85	1748.5	109.1	3173.56	208.3	4261	292	143.7
	46	673	119	5.66	0.146518	2.333	2.13155	19.11	0.105512	19.808	881.4	19.2	1159.09	132.8	172	364	95.5
	47	954	269	3.54	0.069136	2.197	0.930081	19.144	0.09757	19.79	430.9	9.2	667.68	93.9	1578	370	266.2
	48	720	124	5.82	0.126937	2.791	6.489944	19.296	0.370811	19.661	770.4	20.3	2044.54	171.4	3795	298	392.6
	49	205	157	1.3	0.174766	2.275	1.657301	13.228	0.068777	13.322	1038.3	21.8	992.34	84	892	275	-14.1
	50	559	497	1.12	0.081846	1.901	1.350469	17.883	0.119671	17.917	507.1	9.3	867.76	104.7	1951	320	284.8
	51	998	217	4.6	0.145536	2.223	1.698233	17.35	0.08463	17.328	875.9	18.2	1007.87	111.3	1307	336	49.2
	52	2324	1016	2.29	0.062278	3.52	1.792381	17.721	0.208735	18.461	389.5	13.3	1042.69	116	2896	299	643.5
	53	258	361	0.71	0.070896	2.552	0.872145	20.878	0.089221	17.983	441.6	10.9	636.73	99.1	1409	344	219.1
	54	708	81	8.7	0.146136	2.715	1.356741	10.996	0.067335	11.067	879.3	22.3	870.47	64.4	848	230	-3.5
	55	569	376	1.51	0.16208	5.053	13.18118	6.567	0.589826	4.137	968.3	45.4	2692.71	62.1	4483	60	363
	56	545	199	2.74	0.244396	7.509	6.366504	7.435	0.188932	4.243	1409.5	95.1	2027.66	65.3	2733	70	93.9

Cone. (ppm)				Ratios								Ages				
Spot	[U]	[Th]	U/Th	$^{206}\text{Pb} / ^{238}\text{U}$	$2\sigma$	$^{207}\text{Pb} / ^{235}\text{U}$	$2\sigma$	$^{207}\text{Pb} / ^{230}\text{Pb}$	$2\sigma$	$^{206}\text{Pb} / ^{238}\text{U}$	$2\sigma$	$^{206}\text{Pb} / ^{238}\text{U}$	$2\sigma$	$^{206}\text{Pb} / ^{238}\text{U}$	$2\sigma$	% Disc
57	729	99	7.36	0.117819	5.226	3.5404	7.473	0.217939	4.953	718	35.5	1536.29	59.2	2966	80	313
58	620	60	10.35	0.147654	5.423	2.405237	4.065	0.118144	5.608	887.8	45	1244.16	29.2	1928	100	117.2
59	556	67	8.28	0.161497	7.712	1.846465	4.045	0.082923	9.737	965.1	69.1	1062.17	26.6	1267	190	31.3
60	1438	468	3.07	0.072798	8.824	1.195211	8.62	0.119076	14.397	453	38.6	798.37	47.7	1942	257	328.8
61	1381	499	2.77	0.069516	8.867	0.671339	5.891	0.070041	13.026	433.2	37.2	521.53	24	930	267	114.6
62	280	181	1.55	0.345443	8.979	5.290373	4.667	0.111073	12.214	1912.8	148.6	1867.31	39.9	1817	222	-5
63	446	286	1.56	0.086646	8.927	2.15955	8.72	0.180764	13.827	535.7	45.9	1168.13	60.6	2660	229	396.6
64	402	136	2.95	0.23096	9.775	11.994079	21.272	0.376643	23.559	1339.5	118.2	2603.94	202	3818	356	185.1
65	420	98	4.29	0.173116	9.707	4.636628	25.937	0.194252	27.728	1029.3	92.3	1755.89	220	2778	455	170
66	938	143	6.56	0.157558	9.72	6.080174	23.729	0.279882	26.11	943.2	85.3	1987.41	209.9	3362	408	256.5
67	462	128	3.6	0.16037	9.658	1.488795	23.587	0.06733	26.086	958.8	86	925.82	144.2	848	542	-11.6
68	375	139	2.69	0.087634	9.771	71.885499	23.746	0.156046	26.266	541.5	50.8	1076	158.8	2413	446	345.6
69	564	75	7.54	0.095057	7.213	0.780557	27.838	0.059555	30.537	585.4	40.4	585.8	124.5	587	663	0.4
70	1353	302	4.48	0.087217	5.777	4.346637	28.966	0.361452	31.434	539.1	29.9	1702.26	243.7	3756	477	596.8
71	797	318	2.51	0.069064	4.762	0.955402	27.756	0.100331	31.071	430.5	19.8	680.91	138.6	1630	578	278.7
72	421	286	1.47	0.076549	4.886	1.147678	28.491	0.108738	31.62	475.5	22.4	776.15	155.8	1778	577	274
73	920	451	2.04	0.217946	4.983	2.778964	27.175	70.092477	30.633	71271	57.5	1349.9	205.7	1477	581	16.2
74	270	111	2.44	0.105169	4.195	4.235632	6.747	0.292098	6.342	644.6	25.7	1680.95	55.5	3429	99	431.9
75	1101	89	12.31	0.164997	4.395	3.248147	5.284	0.142777	8.455	984.5	40.1	1468.73	41	2261	146	129.7
76	285	123	2.32	0.160368	4.669	2.57749	4.712	0.116568	5.712	958.8	41.6	1294.27	34.5	1904	103	98.6
77	1713	63	27.05	0.077805	4.799	1.98221	11.144	0.184774	10.479	483	22.3	1109.47	75.3	2696	173	458.2
78	224	168	1.33	0.343303	4.323	4.9129	4.282	0.103791	5.691	1902.5	71.2	1804.47	36.1	1693	105	-11
79	392	170	2.3	0.078036	3.889	1.072407	16.377	0.09967	16.817	484.4	18.1	739.92	86.3	1618	313	234
80	1039	101	10.33	0.164275	4.363	5.310938	16.05	0.234476	18.544	980.5	39.7	1870.62	138	3083	296	214.4
81	201	179	1.12	0.085856	5.17	4.437685	17.386	0.374874	18.871	531	26.4	1719.4	145.1	3811	286	617.8
82	742	139	5.34	0.13744	4.465	1.21441	16.007	0.064084	18.287	7830.2	34.8	807.22	89.4	744	387	-10.3
83	936	57	16.43	0.079559	5.821	0.62112	16.465	0.056622	18.296	7493.5	27.7	490.55	64.2	477	405	-3.4
84	535	305	1.75	0.17847	6.735	3.991072	23.645	0.16219	26.081	71058.6	65.8	1632.38	194.3	2479	440	134.1
85	196	174	1.13	0.313688	4.417	7.804408	20.729	0.180443	23.79	1758.8	68	2208.71	188.7	2657	394	51.1
86	296	167	1.78	0.198083	6.261	3.025179	20.85	0.110765	24.161	1165	66.7	1413.99	160.4	1812	439	55.5
87	367	417	0.88	0.406272	4.246	0.841557	20.72	0.157838	23.709	2197.9	79.1	2321.79	191.2	2433	402	10.7

Cone.	Ratios										Ages					
	Spot	[U]	[Th]	U/Th	$^{206}\text{Pb} / ^{238}\text{U}$	$2\sigma$	$^{207}\text{Pb} / ^{235}\text{U}$	$2\sigma$	$^{207}\text{Pb} / ^{230}\text{Pb}$	$2\sigma$	$^{206}\text{Pb} / ^{238}\text{U}$	$2\sigma$	$^{206}\text{Pb} / ^{238}\text{U}$	$2\sigma$	$^{206}\text{Pb} / ^{238}\text{U}$	$2\sigma$
88	1016	672	1.51	0.114808	4.21	1.002011	20.692	0.063299	23.739	700.6	28	704.83	105.5	718	504	2.5
89	864	111	7.79	0.165469	4.212	7.840708	21.043	0.343666	23.864	987.1	38.6	2212.89	191.7	3679	364	272.7
90	2494	175	14.22	0.123734	2.346	5.129	10.683	0.300637	10.458	752	16.6	1840.92	91	3474	162	361.9
91	101	5111.94	0.25643	5.609	12.853556	16.28	0.363541	12.969	1471.6	73.8	2668.98	154.6	3765	197	155.8	
92	731	14	52.02	0.0709	2.272	0.566148	10.308	0.057914	10.394	441.6	9.7	455.52	37.9	527	228	19.2
93	704	491	1.43	0.074871	2.482	1.94553	14.103	0.188462	13.394	465.4	11.1	1096.91	94.9	2729	221	486.3
94	494	357	1.38	0.075121	2.324	0.869466	11.852	0.083944	11.661	7466.9	10.5	635.28	56	1291	227	176.5
95	1284	45	28.74	0.077402	3.306	1.478211	6.985	0.138511	6.341	480.6	15.3	921.5	42.3	2209	110	359.6
96	1016	245	4.14	0.178887	3.817	2.21454	4.297	0.089785	2.026	1060.9	37.3	1185.65	30.1	1421	39	33.9
97	487	257	1.9	0.071885	3.646	0.58713	4.304	0.059237	3.322	447.5	15.8	469.03	16.2	576	72	28.7
98	862	533	1.62	0.076751	3.361	0.959132	4.879	0.090635	3.938	476.7	15.4	682.85	24.3	1439	75	201.9
99	438	6	70.5	0.075979	3.281	1.272554	4.997	0.121474	3.92	472.1	14.9	833.56	28.4	1978	70	319
100	861	223	3.86	0.18892	3.642	2.854378	4.133	0.109581	3.083	1115.5	37.3	1369.96	31.1	1792	56	60.7
101	2484	948	2.62	0.096177	4.194	5.10619	10.685	0.385058	8.788	592	23.7	1837.14	91	3852	133	550.7
102	1803	1383	1.3	0.090538	4.143	3.918445	10.329	0.313893	8.115	558.7	22.2	1617.5	83.7	3540	125	533.6
103	756	127	5.94	0.122417	3.555	2.399164	5.068	0.14214	4.927	744.5	25	1242.35	36.3	2253	85	202.7
104	1420	12	114.21	0.069016	2.847	0.628404	4.772	0.066058	4.127	430.2	11.8	495.23	18.7	808	86	87.9
105	716	1186	0.6	0.13622	2.563	1.364309	4.416	0.072639	3.472	823.3	19.8	873.72	25.9	1004	70	21.9
106	910	163	5.58	0.204702	2.877	8.258559	7.617	0.292604	5.347	1200.5	31.5	2259.78	69.1	3432	83	185.8
107	441	323	1.36	0.104968	5.017	4.726349	13.17	0.326562	8.598	643.5	30.7	1771.92	110.8	3601	132	459.6
108	604	37	16.3	0.103042	2.308	0.827822	2.281	0.058267	1.675	632.2	13.9	612.4	10.5	540	37	-14.6
109	662	230	2.88	0.135549	2.066	1.755993	5.669	0.093956	4.916	819.4	15.9	1029.37	36.7	1507	93	83.9
110	796	214	3.73	0.14601	2.832	3.079769	21.913	0.15298	20.716	878.6	23.3	1427.67	169.5	2380	353	170.8
111	371	97	3.82	0.181577	5.18	5.466607	28.919	0.218352	26.233	1075.6	51.3	1895.37	253.4	2969	423	176
112	1415	4	380.5	0.069608	3.44	0.507351	26.554	0.052863	24.96	433.8	14.4	416.67	91	323	567	-25.6
113	274	76	3.61	0.146756	5.172	3.273384	27.049	0.161771	24.99	882.8	42.7	1474.75	213.5	2474	422	180.3
114	265	252	1.05	0.09327	4.005	2.897183	28.346	0.225286	25.816	574.8	22	1381.18	217.2	3019	414	425.2
115	713	75	130.58	0.072156	3.398	0.812671	26.919	0.081685	25.401	449.1	14.7	603.95	123.1	1238	498	175.6

## APPENDIX E-Zircon Data Tables

**Table E.1: 7-1-02-10**

Cone. (ppm)				Ratios								Ages				
Spot	[U]	[Th]	U/Th	$^{206}\text{Pb} / ^{238}\text{U}$	$2\sigma$	$^{207}\text{Pb} / ^{235}\text{U}$	$2\sigma$	$^{207}\text{Pb} / ^{230}\text{Pb}$	$2\sigma$	$^{206}\text{Pb} / ^{238}\text{U}$	$2\sigma$	$^{206}\text{Pb} / ^{238}\text{U}$	$2\sigma$	$^{206}\text{Pb} / ^{238}\text{U}$	$2\sigma$	%Disc
1	161	338	0.48	0.0728	3.431	0.60332	15.945	0.0600	14.601	453.1	15	479.34	61	607	316	33.9
2	194	294	0.66	0.0649	3.254	0.6675	16.246	0.0745	15.497	405.5	12.8	519.22	66.1	1057	312	160.7
4	128	215	0.6	0.0740	3.9	0.5768	19.395	0.0564	17.589	460.7	17.3	462.45	72.2	471	389	2.3
5	164	394	0.42	0.0718	4.492	0.8059	25.705	0.0813	23.438	447.2	19.4	600.18	117	1230	460	175.1
6	125	444	0.28	0.07416	3.679	0.9660	21.065	0.0944	19.41	461.2	16.4	686.45	105.5	1518	366	229
7	141	820	0.17	0.09560	7.032	3.3330	29.531	0.25283	25.209	588.6	39.6	1488.82	234.7	3203	399	444.1
8	169	418	0.4	0.070288	3.635	0.73107	24.899	0.07543	23.186	437.9	15.4	557.18	107.2	1080	465	146.7
9	98	227	0.43	0.071409	3.739	0.544271	24.556	0.055279	22.791	444.6	16.1	441.24	88.1	424	509	-4.7
10	169	435	0.39	0.071559	3.737	0.627377	24.54	0.063586	22.796	445.5	16.1	494.46	96.4	728	483	63.4
11	295	659	0.45	0.069768	3.61	0.699377	25.014	0.072703	23.342	434.8	15.2	538.42	104.9	1006	474	131.3
12	80	205	0.39	0.07435	3.437	0.632422	24.833	0.061691	23.638	462.3	15.3	497.6	98	663	506	43.5
13	75	133	0.56	0.505943	4.005	12.742276	31.673	0.18266	29.923	2639.3	86.8	2660.79	307.2	2677	495	1.4
14	100	148	0.68	0.07868	3.998	0.752844	32.03	0.069397	30.378	488.2	18.8	569.87	140.6	911	625	86.5
15	65	295	0.22	0.07212	4.066	0.596289	31.817	0.059965	30.044	448.9	17.6	474.88	121.3	602	650	34.2
16	217	666	0.33	0.27636	3.076	4.445219	20.345	0.116659	19.105	1573	42.9	1720.81	170.2	1906	343	21.1
17	65	164	0.4	0.093848	5.14	2.519171	27.402	0.194684	24.337	578.3	28.4	1277.58	201.8	2782	399	381.1
18	59	298	0.2	0.168919	4.393	2.498627	31.499	0.107281	29.041	1006.2	40.9	1271.64	232.4	1754	531	74.3
19	123	704	0.17	0.139362	4.554	2.224233	32.45	0.115754	29.417	841.1	35.9	1188.7	231.2	1892	529	124.9
20	59	116	0.51	0.171816	4.382	2.313086	31.803	0.09764	29.11	1022.1	41.4	1216.31	229.3	1580	545	54.5
21	168	373	0.45	0.069925	3.166	0.880349	23.073	0.091311	20.861	435.7	13.3	641.17	110.1	1453	397	233.5
22	27	174	0.15	0.15833	3.241	6.57163	22.321	0.30103	20.309	947.5	28.6	2055.55	199.2	3476	314	266.8

Spot	Cone. (ppm)				Ratios						Ages					
	[U]	[Th]	U/Th	$^{206}\text{Pb} / ^{238}\text{U}$	$2\sigma$	$^{207}\text{Pb} / ^{235}\text{U}$	$2\sigma$	$^{207}\text{Pb} / ^{230}\text{Pb}$	$2\sigma$	$^{206}\text{Pb} / ^{238}\text{U}$	$2\sigma$	$^{206}\text{Pb} / ^{238}\text{U}$	$2\sigma$	$^{206}\text{Pb} / ^{238}\text{U}$	$2\sigma$	%Disc
23	131	572	0.23	0.130312	2.744	1.462805	12.903	0.081414	11.965	789.6	20.4	915.17	78	1231	235	56
24	82	79	1.03	0.074749	2.262	0.739513	18.034	0.071753	16.411	464.7	10.1	562.12	78	979	334	110.7
25	153	664	0.23	0.072337	2.657	0.968779	18.575	0.097132	16.601	450.2	11.6	687.83	93.1	1570	311	248.7
26	104	387	0.27	0.074964	2.283	0.682261	11.14	0.066008	10.888	466	10.3	528.14	45.9	807	228	73.1
27	26	133	0.2	0.311807	1.962	4.70883	10.883	0.109528	9.99	1749.6	30.1	1768.81	91.4	1792	182	2.4
28	88	92	0.96	0.155394	2.157	1.715317	13.413	0.080059	12.503	931.1	18.7	1014.28	86.2	1198	247	28.7
29	76	227	0.34	0.488852	1.94	10.90704	16.695	0.161819	15.356	2565.7	41.1	2515.24	156.5	2475	259	-3.5
30	159	475	0.34	0.072866	2.596	0.667245	17.393	0.066414	15.81	453.4	11.4	519.04	70.8	819	330	80.7
31	200	240	0.83	0.071866	2.25	0.701234	11.274	0.070768	10.492	447.4	9.7	539.53	47.2	951	215	112.5
32	165	219	0.75	0.525503	2.231	16.438704	13.382	0.226877	12.292	2722.5	49.5	2902.67	128.8	3030	197	11.3
33	322	699	46	0.068879	2.174	0.51571	2.519	0.054302	1.353	429.4	9	422.28	8.7	384	30	-10.7
34	70	447	0.16	0.175519	2.569	2.109497	5.983	0.087167	5.129	1042.4	24.7	1151.91	41.2	1364	99	30.9
35	98	249	0.39	0.186531	6.158	4.382672	11.627	0.170407	5.698	1102.6	62.4	1709.08	96.4	2562	95	132.3
36	49	145	0.34	0.490545	1.997	11.242917	3.437	0.166226	2.832	2573	42.4	2543.48	32.1	2520	48	-2.1
37	284	560	0.51	0.091813	4.689	3.352979	12.484	0.264865	8.248	566.3	25.4	1493.49	97.9	3276	130	478.75
38	28	145	70.19	0.361498	2.191	10.620872	5.913	0.213085	4.864	1989.3	37.5	2490.53	54.9	2929	79	47.2
39	352	1611	0.22	0.06947	2.257	1.089985	5.489	0.113794	4.919	433	9.5	748.5	29.1	1861	89	329.8
40	226	893	0.25	0.070445	2.574	1.181627	9.223	0.121654	7.238	438.8	10.9	792.07	50.8	1981	129	351.3
41	84	251	0.33	0.078971	2.359	1.068115	4.699	0.098095	4.326	490	11.1	737.82	24.6	1588	81	224.1
42	104	257	0.4	0.075454	2.223	0.575253	2.94	0.055294	2.929	468.9	10.1	461.41	10.9	424	65	-9.6
43	256	371	0.69	0.072493	2.156	0.889158	9.301	0.088957	9.105	451.2	9.4	645.92	44.5	1403	174	211
44	81	247	0.33	0.409554	4.035	10.133341	7.995	0.179448	4.779	2212.9	75.6	2447.02	74	2648	79	19.7
45	350	742	0.47	0.073902	2.832	0.715459	4.001	0.070215	3.333	459.6	12.6	547.98	16.9	935	68	103.4
46	165	368	0.45	0.072737	2.33	0.815124	9.169	0.081277	9.351	452.6	10.2	605.32	41.8	1228	184	171.3
47	329	1157	0.28	0.065642	1.994	0.835333	8.267	0.092294	8.67	409.8	7.9	616.57	38.2	1473	165	259.5
48	148	387	0.38	0.07659	2.468	0.880999	11.921	0.083426	11.517	475.7	11.3	641.52	56.8	1279	224	168.9
49	441	4370	0.1	0.220579	2.443	3.963092	9.688	0.130307	9.681	1284.9	28.5	1626.67	78.7	2102	170	63.6
50	111	308	0.36	0.071724	2.261	0.549265	9.681	0.055541	9.767	446.5	9.8	444.51	34.9	434	218	-2.8
51	312	1115	0.28	0.072962	2.306	0.738042	7.208	0.073364	7.599	454	10.1	561.26	31.1	1024	154	125.6

Cone.	(ppm)	Ratios										Ages				
		Spot	[U]	[Th]	U/Th	$^{206}\text{Pb} / ^{238}\text{U}$	$2\sigma$	$^{207}\text{Pb} / ^{235}\text{U}$	$2\sigma$	$^{207}\text{Pb} / ^{230}\text{Pb}$	$2\sigma$	$^{206}\text{Pb} / ^{238}\text{U}$	$2\sigma$	$^{206}\text{Pb} / ^{238}\text{U}$	$2\sigma$	%Disc
52	201	492	0.41	0.071012	1.88	0.639423	7.883	0.065307	7.936	442.2	8	501.95	31.2	784	167	77.3
53	100	301	0.33	0.458198	2.192	9.746931	9.459	0.154281	8.958	2431.6	44.4	2411.15	87.3	2394	152	-1.5
54	204	500	0.41	0.475249	1.981	11.164822	9.409	0.170384	8.923	2506.5	41.1	2536.98	87.9	2561	149	2.2
55	135	226	0.6	0.465132	2.511	10.983793	9.639	0.171267	9.049	2462.2	51.4	2521.76	89.9	2570	151	4.4